RESEARCH ARTICLE

ESPL WILEY

Pronounced increase in slope instability linked to global warming: A case study from the eastern European Alps

Sara Savi[1,2] ⓘ | Francesco Comiti[2] | Manfred R. Strecker[1]

[1]Institute of Geosciences, University of Potsdam, Potsdam, Germany

[2]Faculty of Science and Technology, Free University of Bozen-Bolzano, Bolzano, Italy

Correspondence
Dr Sara Savi, Institute of Geosciences, University of Potsdam, Potsdam, Germany.
Email: savi@geo.uni-potsdam.de

Funding information
Deutsche Forschungsgemeinschaft, Grant/Award Number: 399435624

Abstract

In recent decades, slope instability in high-mountain regions has often been linked to increase in temperature and the associated permafrost degradation and/or the increase in frequency/intensity of rainstorm events. In this context we analyzed the spatiotemporal evolution and potential controlling mechanisms of small- to medium-sized mass movements in a high-elevation catchment of the Italian Alps (Sulden/Solda basin). We found that slope-failure events (mostly in the form of rockfalls) have increased since the 2000s, whereas the occurrence of debris flows has increased only since 2010. The current climate-warming trend registered in the study area apparently increases the elevation of rockfall-detachment areas by approximately 300 m, mostly controlled by the combined effects of frost-cracking and permafrost thawing. In contrast, the occurrence of debris flows does not exhibit such an altitudinal shift, as it is primarily driven by extreme precipitation events exceeding the 75th percentile of the intensity-duration rainfall distribution. Potential debris-flow events in this environment may additionally be influenced by the accumulation of unconsolidated debris over time, which is then released during extreme rainfall events. Overall, there is evidence that the upper Sulden/Solda basin (above ca. 2500 m above sea level [a.s.l.]), and especially the areas in the proximity of glaciers, have experienced a significant decrease in slope stability since the 2000s, and that an increase in rockfalls and debris flows during spring and summer can be inferred. Our study thus confirms that "forward-looking" hazard mapping should be undertaken in these increasingly frequented, high-elevation areas of the Alps, as environmental change has elevated the overall hazard level in these regions.

KEYWORDS
debris flows, frost-cracking, multi-temporal analyses, permafrost, rainfall events, rockfalls, temperature extremes

1 | INTRODUCTION

Since Europe's hot summer of 2003, the awareness and interest of the scientific community regarding the dynamic coupling between global warming and mountain-slope instability has increased significantly (Gruber et al., 2004a; Ravanel et al., 2010), stimulating a broad spectrum of studies that has generally confirmed such a relationship (e.g., Allen & Huggel, 2013; Coe, 2020; Haeberli, 1997, 2010; Haeberli, 2013; Hock et al., 2019; Huggel et al., 2012, and references cited therein). At the same time, the intensive touristic use of high-elevation mountain areas that in recent decades has taken place on a global scale has led to an expansion of infrastructure, thereby increasing the vulnerability of high-mountain areas to the impacts of natural hazards such as rockfalls, earth flows, debris flows, and landslides (Bommer et al., 2010; Coe, 2020; Hock et al., 2019; Ravanel et al., 2013). Although the existence of a link between global warming and rockfall occurrence has been ascertained in several regions (Coe, 2020; IPCC, 2014; Hock et al., 2019), for other mass-movement

phenomena, such as debris flows and complex landslides, this relationship is not so certain (Huggel et al., 2012). In light of the predictions regarding future climatic trends and their impact on high-elevation regions (e.g., Gobiet et al., 2014; IPCC, 2014), a better understanding of the relationships between recent climate change and slope stability is thus of primary importance to properly anticipate future expansion of hazardous areas and to mitigate any associated risks (e.g., Coe, 2020; Haeberli et al., 1997; Hock et al., 2019, and references cited therein).

For the Alps in particular, permafrost degradation (e.g., Draebing et al., 2017a; Haeberli, 2013; Huggel et al., 2012; Noetzli & Gruber, 2009; Ravanel et al., 2013), ice segregation (e.g., Draebing & Krautblatter, 2019; Fischer et al., 2012; Girard et al., 2013; Hasler et al., 2011; Krautblatter et al., 2013; Murton et al., 2001), and a higher frequency of extreme precipitation events (e.g., Hock et al., 2019; Krautblatter & Moser, 2009; Paranunzio et al., 2019) have been argued to be responsible for increased slope-failure events over the last decades. Although extensive research into these topics has been conducted, the complexity of the interactions between climatic forcing and soil/bedrock parameters (i.e., ground temperature, snow cover, surface topography, etc.) still challenges our understanding of the mechanisms triggering slope failures, hence limiting our ability to predict mountain-slope instability (Beniston et al., 2018; Damm & Felderer, 2013; Fischer et al., 2012; Huggel et al., 2012). In this respect, the main challenges we face can be summarized as follows: (i) databases of natural extreme events are often incomplete (e.g., Allen & Huggel, 2013; Marchi et al., 2019; Sass & Oberlechner, 2012); (ii) a time lag may exist between the impact of climatic forcing and the failure event (e.g., Crozier, 2010; Haeberli & Beniston, 1998; Huggel et al., 2012; Noetzli & Gruber, 2009); (iii) ground surface temperature and soil water content are often unknown at regional scales (e.g., Gruber et al., 2004b; Gubler et al., 2013; Luetschg & Haeberli, 2005); and (iv) the role of snow cover/snow depth has not yet been clarified (e.g., Draebing et al., 2014, 2017a, 2017b; Harris & Conte, 1992; Salzmann et al., 2007; Staub & Delaloye, 2017; Zhang, 2005). Each of the these aspects is briefly discussed later.

Firstly, while databases for large landslides and rock avalanches tend to be more complete and cover longer time periods (Eisbacher & Clague, 1984; Porter & Orombelli, 1981), the quality of the database for small- to medium-scale events may depend on available recording technologies, on when and where the event occurred (i.e., low/high altitude; season during which witnesses were present or not), and on whether damage to infrastructure or human losses were caused (Allen & Huggel, 2013). Furthermore, the recent increase in awareness of these natural events, in the application of new technologies, and in the intensive use of high-elevation areas may cause these databases to be inherently biased toward events that have taken place in recent decades (Cavalli et al., 2017; Marchi et al., 2019, 2020; Sass & Oberlechner, 2012).

Secondly, in terms of a time lag between the event and its trigger mechanism, a direct connection between recent global warming and slope instability in high mountains is generally difficult to assess, because slope failures are often only indirectly linked to specific climate-related trends (Crozier, 2010; Huggel et al., 2012; IPCC, 2014). Slope failures related to permafrost degradation or to extreme rainfall events may differ significantly in form and timing. For example, an intense rainfall event or repeated episodes with high rainfall can be more reliably linked to slope movements because of the short time needed to increase pore pressure to the critical level for failure (e.g., Krautblatter & Moser, 2009). In contrast, the direct link between increasing temperature and slope instability in high-elevation permafrost areas may be masked by a lag-time effect between the melting and the destabilization of frozen ground (Haeberli & Beniston, 1998; Noetzli & Gruber, 2009). Previous studies have reported that this phenomenon is particularly true for large landslides and rock avalanches, with failure planes at greater depths within bedrock, similarly to what has been observed in the context of glacial debuttressing (e.g., Haeberli et al., 2013; Huggel et al., 2012). The time needed to destabilize these slopes may be on the order of decadal to millennial timescales (Haeberli & Beniston, 1998; Hasler et al., 2012; Matsuoka et al., 1998; Noetzli & Gruber, 2009; Wegmann et al., 1998). In contrast, small- to medium-sized events, whose detachment surfaces are closer to the surface, may reflect a more direct reaction to environmental change and be more easily ascribed to climatic extremes (Allen & Huggel, 2013; Crozier, 2010; Huggel et al., 2012; Matsuoka et al., 1998; Paranunzio et al., 2019).

With regard to the third point mentioned earlier, ground-surface temperature and water content significantly influence slope stability by affecting heat transfer and bedrock fracturing (Davies et al., 2001; Draebing et al., 2014; Krautblatter et al., 2013; Murton et al., 2006; Noetzli & Gruber, 2009; Rode et al., 2016). Surface temperatures can differ substantially from air temperatures (Haeberli et al., 2010; Gubler et al., 2013; Zhang, 2005) and are generally monitored at a limited number of locations. Although remote sensing may provide information on ground conditions (e.g., Bertoldi et al., 2010; Sánchez-Aparicio et al., 2020; Sobrino et al., 2020), the spatial resolution of satellite-derived estimates on temperature is insufficient, especially for rugged, topographically high areas where surface temperatures need to be known in greater detail (Beniston et al., 2018; Gruber et al., 2004b). Alternatively, numerical models may be useful in estimating ground-surface temperatures with a precision within a few degrees Celsius (Gruber et al., 2004b; Gubler et al., 2013; Li et al., 2019; Salzmann et al., 2007; Stocker-Mittaz et al., 2002). However, these models require atmospheric input parameters (e.g., solar irradiance, wind speed and direction, air and vapor pressure) that have a large spatiotemporal variability and that may not be available for every weather station in a specific region.

Finally, snow cover also exerts a strong effect on ground temperatures by increasing albedo, long-wave emissivity and absorptivity, and by decreasing thermal conductivity (McColl & Draebing, 2019; Zhang, 2005). The morphology and topography of steep mountainous terrains cause snow depths to be extremely variable in terms of time and space (Draebing et al., 2017a; Hasler et al., 2011; Staub & Delaloye, 2017), which changes ground thermal conditions locally. In general, when viewed at annual timescales, a thick snow cover (e.g., snow thickness > 60–80 cm; Luetschg & Haeberli, 2005; Staub & Delaloye, 2017) prevents the ground from cooling and protects the soil layer from cold air temperatures during winter (Zhang, 2005), thus causing mean annual ground-surface temperatures (MAGSTs) to be several degrees higher than air temperatures. Conversely, thin snow cover may decrease ground temperatures (Hasler et al., 2011) and expose the ground surface to severe frost conditions (Zhang, 2005). Importantly, both the duration and the beginning and end of the

snow-cover season influence the interactions between air and ground temperatures (Luetschg & Haeberli, 2005). If snow falls late in autumn, for example, the protective effect of snow cover on ground temperatures is reduced, whereas during those years with relatively short-lived snow cover, ground temperatures may be lower than air temperatures (Zhang, 2005).

In light of these forcing factors driving the destabilization of steep mountain slopes, it is clear that temperature change and extreme rainfall events both play a pivotal role in the spatial and temporal distribution of high-elevation mass-movement events and sediment transfer. Under the specter of recent climate change and the apparent worldwide increase of mass movements in high mountains (Hock et al., 2019), we therefore set out to analyze spatial and temporal patterns of slope instability in a catchment of the Italian Alps, from where climate-related mass movements have been reported (e.g., Fischer et al., 2006, 2012; Huggel et al., 2012; Paranunzio et al., 2019; Ravanel et al., 2013; Schlögel et al., 2020). By taking advantage of the rich climate data, local mass-movement inventories, and high-resolution topographic information available from the Autonomous Province of Bozen/Bolzano, our analysis primarily focuses on deciphering areas of landslide initiation (hereafter referred to as detachment points). The detachment points are identifiable at different scales in the field and on orthophotos, which are available for the study site as of 1945.

Here, we restrict ourselves to small- to medium-sized detachments (e.g., break-off scars of a few square meters) that generally initiate small- to medium-sized rockfalls, slides, and debris flows. The type of process generated after an initial detachment depends on several factors that may include: (i) the slope of the detachment point; (ii) the possible entrainment of additional material once motion has started; and (iii) the amount of water involved. The type of instability is therefore influenced by the location of the detachment point in relation to its geomorphic domain. Consequently, rockfalls will occur on rockwalls and slides on more gentle, soil-covered slopes, whereas debris flows will be mainly generated within areas with steep channels and unconsolidated sediment. The principal hypothesis that we set out to test in this context is that climate warming reduces slope stability and causes a shift in the location of the detachment points toward higher elevations. Such a transition toward higher elevations would mainly reflect the rise in temperature and its effects on the ground thermal regime, with associated permafrost thaw, ice segregation, and frost-cracking mechanisms. In contrast, intense rainfall events – which are predicted to increase in magnitude and/or frequency as a consequence of global warming (Ban et al., 2015; Jacob et al., 2018) – may not reveal a similar altitudinal shift, since the mechanisms governing slope instability are primarily linked to the duration and intensity of a rainfall event (Berti et al., 2020). Therefore, in this study we analyzed multi-decadal variations both in air temperature – with its related effects of the ground thermal regime – and in precipitation. By employing a thermal model we used the measured temperatures to analyze the mechanisms that govern ice segregation and infer its possible role in fracturing bedrock. To address potential links between precipitation, temperature, and mass movements, we used data from two weather stations located within our study area and analyzed rainfall extreme events and temperature anomalies, as well as the possible influence of snow cover on water availability and slope stability.

Finally, we investigated where most changes in slope stability occurred.

2 | STUDY AREA

We analyzed the upper Sulden/Solda river basin (drainage area 76 km^2 upstream from the confluence with the Trafoi River, near the village of Gomagoi, 1275 m above sea level [a.s.l.]) located in the eastern Italian Alps, in the western portion of the Vinschgau/Val Venosta valley (South Tyrol, Figure 1). The basin comprises some of the highest peaks of the region, including the Ortler/Ortles (3905 m a.s.l.). The bedrock geology of the basin is dominated by the Paleozoic low-grade metamorphic units of the Austroalpine domain (Campo nappe, with the *Zebrù tectonic sliver* separated by the Zebrú and the Madritsch thrust faults), which constitute the central and eastern slopes of the catchment area (Figure 1a). These units are mainly composed of quartz phyllites, mica schists, and paragneisses and orthogneisses (ISPRA, 2012). Metamorphic rocks also crop out in the northern sector of the catchment, where they belong to the Permian orthogneisses of the Lasa unit (ISPRA, 2012). On the western side of the basin, and at higher altitudes, limestones and dolomites of the Ortles nappe are exposed. The rocks exhibit different degrees of metamorphism, folding, jointing, and fractures that are mainly related to the Eo-Alpine phase of thrusting and subsequent deformation (ISPRA, 2012).

The faults and fractures associated with the tectono-stratigraphic units largely controls the morphology of the landscape, defining the relief and the orientation of main valleys and ridges. The pervasive system of joints is one of the responsible factors that influence slope failures leading to unconsolidated talus on steep slopes (ISPRA, 2012). In the Sulden basin this structural control is reflected by steeper debris-flow tributaries with highest peaks located to the west, and a more gentle morphology with larger tributaries and lower peaks to the east. A detailed geomorphic map can be found in Buter et al. (2020) (Figure 1b) and was used to analyze the landforms of the areas that constitute the source of instability. The upper portion of the basin contains several glaciers (Figure 1c). Based on official glacier inventories (Province of Bozen/Bolzano, 2012; Valentini, 1985), the glaciated area in 1982 covered ca. 12% (11.6 km^2) of the basin, whereas in 2006 it had decreased to 9.4% (ca. 9 km^2). By 2017, based on orthophoto mapping, satellite-based multispectral band analysis, and a multi-temporal coherence mosaic obtained by Sentinel-1 time series (courtesy of the Institute for Earth Observation of the EURAC research center, Bozen; Barella et al., 2020), the glacier extent had further diminished to 7.5% (ca. 7.2 km^2). Glaciers have also been reduced in volume (Carturan et al., 2013), thus exposing bedrock and steep rockwalls at high elevations.

For the climatic reference period 1981–2010, mean annual air temperature (MAAT) at the Sulden/Solda village (hereafter, Sulden station at 1907 m a.s.l.) was 2.8°C, whereas mean annual precipitation (MAP) averaged to 835 mm (3PClim database; http://www.3pclim.eu/). Importantly, the basin hosts a second weather station at an altitude of 2825 m a.s.l. (hereafter, Madritsch station), for which climatic reference values (period 1981–2010) were −2.4°C
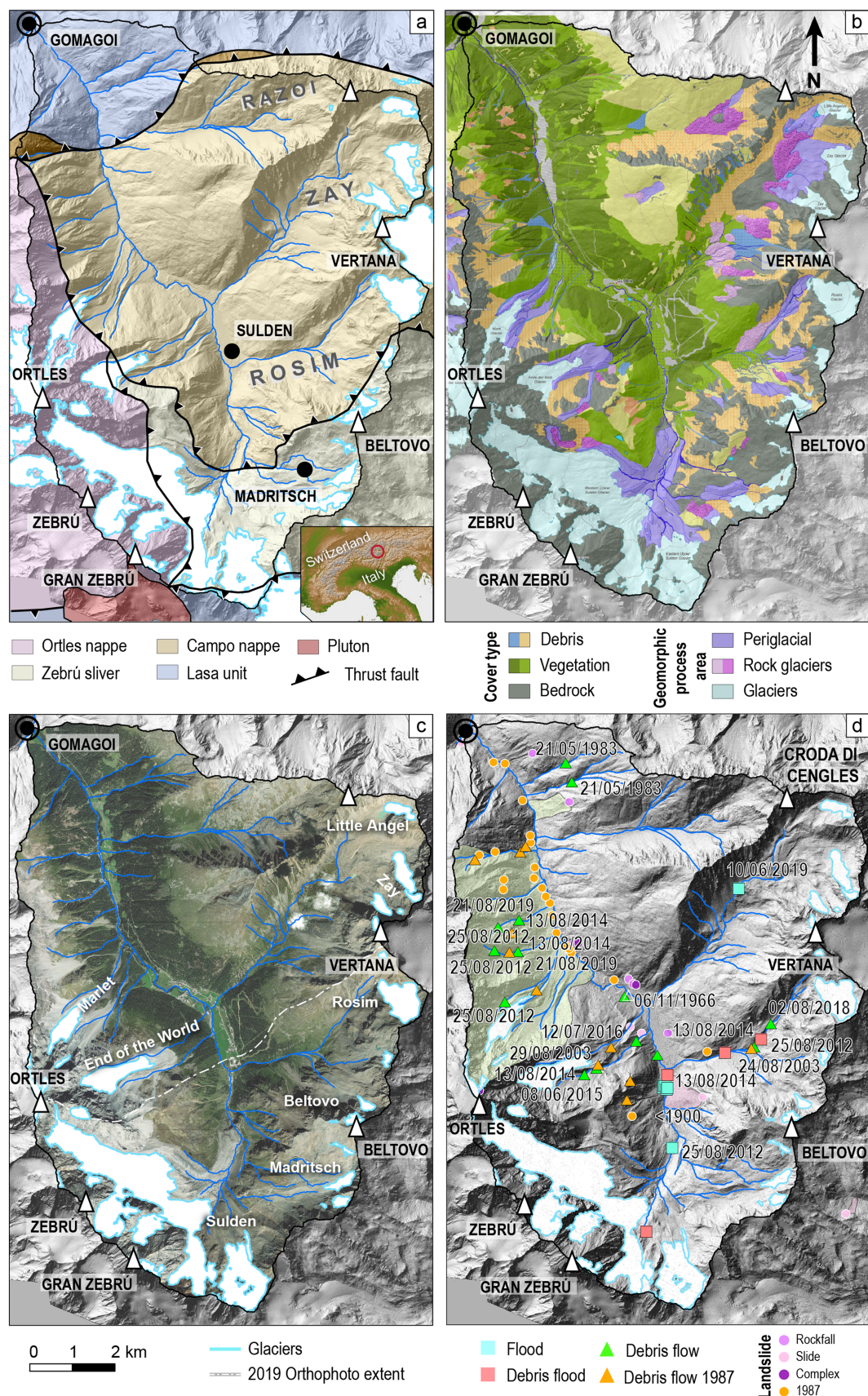
FIGURE 1 Detailed maps of the study area: (a) geology (Autonomous Province of Bozen); (b) geomorphology (for details of the different landforms and processes refer to Buter *et al.*, 2020); (c) orthophoto taken in 2017 with glacier extent and hydrographic network; (d) natural-hazard phenomena reported in the database of the Autonomous Province of Bozen and Schiona (1994). Dates refer to debris-flow and debris-flood events. Green areas refer to regions prone to debris flows; pink areas indicate rotational slides [Color figure can be viewed at wileyonlinelibrary.com]

for the MAAT and 980 mm for the MAP, respectively (3PClim database).

3 | MATERIALS AND METHODS

3.1 | Location of detachment points

Aerial photographs and orthophotos from various sources (i.e., Italian Military Geographic Institute, Autonomous Province of Bozen, Free University of Bozen) spanning from 1945 to 2019 have been used to locate the different detachment points. More information on the photographs used can be found in Section S1 of the Supporting Information. Deciphering the detachment points through orthophotos and aerial photographs (hereafter referred to as orthophotos for simplicity) partially solves the problem of not having a complete list of historical mass-movement events, because the same approach can be used for both recent and past landscape characteristics. Moreover, this method has the advantage of being able to cover very remote areas, such as rockwalls in the high-elevation sectors of the basin and the boundaries between bedrock and glaciers. In addition to studying the orthophotos, we inspected detachment points during field campaigns in 2019 and were able to add the locations of several slope failures and initiation points of debris flows with respect to storm events in 1987 derived from the detailed map of Schiona (1994). Detachments were defined based on age-dependent color differences in the bedrock, indicating exposure and removal of bedrock due to recent mass wasting (e.g., Krautblatter et al., 2012; Stötter, 1994). In order to assess any possible bias associated with the quality of the different images, we performed an image-quality check based on two main components: (i) the Natural Image Quality Evaluator (NIQE) algorithm (Mittal et al., 2013), and (ii) the percentage of shadows and fresh snow cover that were present on each image. Based on the results of the quality check, we combined the individual detachment points of the 2014 and 2016 images and those of the 2017 and 2018 orthophotos (more details can be found in the Supporting Information, Section S1). In most of the orthophotos, snow-cover extent is at its minimum because the images were acquired at the end of the summer season. As such, each time period analyzed includes the summer of the year in which the image was collected, but not the ensuing autumn and winter, which are included in the subsequent time series. Overall, we were able to analyze the following time periods: 1945–1985; 1987; 1985–2003; 2003–2006; 2006–2008; 2008–2011; 2011–2016; 2016–2018; 2018–2019.

The low frequency of old orthophotos (Supporting Information Table S1) may introduce a bias in the number of points detected in the oldest time period (1945–1985), which alone covers a longer time frame than all the other orthophotos combined (i.e., 1985–2019). For the former time span, it is likely that older detachment scars were no longer visible on the orthophotos, thus resulting in an underestimation of the total points. The same problem could be relevant for the time period between 1985 and 2003. However, for this time span, the locations of older detachments were retrieved from the detailed map of Schiona (1994); possible underestimations concerning detachment locations are thus limited with respect to the numerous instabilities associated with the 1987 summer events (Schiona, 1994). Also, 2018–2019 is the period for which orthophoto coverage was only available for the upper portion of the basin (Figure 1c), which could

have resulted in an underestimation in the number of points. However, this underestimation is partially compensated by data retrieved during field surveys conducted by us in the lower part of the basin in summer 2019.

3.2 | Analysis of climate data

To analyze the climatic variability of the basin, we used the data from the two weather stations located within the catchment, Sulden and Madritsch (Figure 1a). The Sulden station has been recording data with high resolution (i.e., 10 min for temperature, and 5 min for precipitation) since 1987, but low-resolution data (e.g., daily) can be retrieved back to 1971 for temperature, and to 1926 for precipitation (the oldest data is, however, often incomplete). The Madritsch station has been registering temperature as well as snow depth (10 min) since 2000 and precipitation (5 min) at high resolution since 2009. In order to homogenize the analysis of climatic trends and anomalies and extend them back in time (i.e., to 1980 at daily resolution, and to 1955 with monthly resolution), we integrated interpolated temperature data provided by the Institute for Earth Observation of the EURAC Research Center, Bozen (Crespi et al., 2020, 2021). More information on this data set and its implementation can be found in the Supporting Information (Section S2).

Snow-cover extent, which is available at daily resolution since 2002, was extracted from MODIS data (EURAC Research Center, Bozen; Matiu et al., 2019; Notarnicola et al., 2011, 2013a, 2013b). Solar irradiance is available from the authorities of the Autonomous Province of Bozen (https://www.tirol.gv.at/statistik-budget/tiris/tiris-anwendungen/solar-tirol/) and is retrieved from satellite data over the period between 2004 and 2013 (Müller et al., 2012). Information on the potential distribution of permafrost in the Sulden basin (Figure 1d) is based on Boeckli et al. (2012) and Kofler et al. (2020) and is supported by field evidence collected during the summer months of 2019 and 2020. Our observations include the occurrence of frozen soil at landslide scars and along talus slopes, as well as measurements of water temperature and electric conductivity at springs.

To analyze temperature extremes and the impact of anomalously hot periods, we used the approach proposed by Paranunzio et al. (2019), which defines periods of temperature extremes as when the daily mean values pass the 95th percentile of the reference daily temperature. The latter is defined annually based on the average of each single day of all available years (e.g., the reference temperature for January 1 is calculated by averaging the temperatures for each January 1 between 1980 and 2019, as this is the period with data at daily resolution). As for the rainfall events that may have triggered debris flows, we used an intensity-duration (I-D) approach (Berti et al., 2020; Caine, 1980; CNR-IRPI, 2010; Guzzetti et al., 2007, 2008). More details on rainfall-event extraction and on the I-D relationships in the Sulden Basin can be found in the Supporting Information (Section S3).

3.3 | Database of events related to natural hazards

The systematic recording of natural hazards in South Tyrol started in 1998 and has been maintained by the Autonomous Province of Bozen

(see also Marchi et al., 2019; Schlögel et al., 2020; Scorpio et al., 2020). The available data indicates that the most common processes in the Sulden catchment are debris flows and debris floods, together with different types of small- to medium-sized landslides (Figure 1d). Debris flows are rather frequent and generally widely distributed. Specifically, major events affecting large portions of the basin occurred on: May 21, 1983; July 19 and August 24, 1987; August 25, 2012; August 13, 2014; and August 21, 2019. We used the data reported in the database of the Bozen Province to evaluate the climatic conditions (i.e., temperature and precipitation) that may have influenced the occurrence of debris flows.

3.4 | Snow-cover effects on slope instability

Draebing et al. (2014) and McColl and Draebing (2019) explained how the combination of bedrock fractures, snow, ice, and water availability may control the thermal gradient in the ground and cause failure through the propagation of fractures in bedrock. In particular, liquid water percolating into fractures may increase the heat transfer through advective processes and lead to ice erosion within the joints (Davies et al., 2001; Draebing et al., 2014; Hasler et al., 2011). As such, meltwater flows on snow-free surfaces can heat the underground by advective transport, contributing to the melting of ice. If water is trapped in bedrock (for example because it is sealed by surrounding frozen ground), it fills the fractures and increases hydrostatic pressure, and eventually (through refreezing during winter) cryostatic pressure (Deline et al., 2015; Draebing et al., 2014). These authors identified two periods of enhanced rock-fall activity, one in early summer and one in autumn (also corresponding to the periods of intense frost wedging observed by Matsuoka, 2001). By using the meteorological data on snow height measured at the Madritsch station, and accounting for the insulating properties of snow (e.g., Zhang, 2005), we used the same approach to find the most probable "instability window" for the Sulden basin.

3.5 | Frost-cracking model

To evaluate the frost-cracking intensity (FCI), we used the model proposed by Hales and Roering (2007), but with modifications by Anderson et al. (2013) and Scherler (2014) to account for the free movement of liquid water, either percolating downward from the surface or migrating upward from depth along the thermal gradient. This is essential as liquid water moving through bedrock fractures is an important means of heat exchange and fundamental for ice-segregation mechanisms (Deline et al., 2015; Draebing et al., 2014; Girard et al., 2013; Krautblatter et al., 2013; Murton et al., 2006; Rode et al., 2016). More details on the model can be found in the Supporting Information (Section S4).

The approach of Hales and Roering (2007) was developed for the calculation of the FCI for a single column of rock and starting from its value of MAAT. Acknowledging the large difference that may exist between air and rock temperature, the authors cautioned that their model calculated frost-cracking intensities in environments dominated by shade. We modified the model to work on the basis of a gridded raster of temperature, thus calculating the FCI for each pixel.

Additionally, as an input parameter we provided a raster representing the MAGST of each time period analyzed (see Figure S5 in the Supporting Information). The MAGST was calculated using a simple approach based on the fact that – for surfaces with little snow cover – ground temperatures are mainly controlled by air temperature and short-wave radiation (Gruber et al., 2004b; Haeberli et al., 2010). As such, we modeled MAGST on a pixel-based approach that combines the relative value of the MAAT raster plus a normalized index obtained by the raster of solar irradiance. More details on our approach and on validation tests can be found in the Supporting Information (Section S5).

4 | RESULTS

4.1 | Detachment-point location

4.1.1 | Geomorphological characteristics

In Figure 2 we show each of the individual detachment points (1017 in total), color-coded according to the different time periods analyzed. The map demonstrates that the oldest detachment points mainly occupy the lower portion of the catchment (e.g., below ca. 2500–2600 m a.s.l.), whereas younger detachments occur at increasingly higher elevations (Figure 3a) with an overall shift of ca. 300 m (see also Section S6 of the Supporting Information). This trend is associated with an increase in the area affected by permafrost, as higher elevations tend to have a more extensive cover of frozen ground (Figure 3b). Similarly, the locations of detachments in terms of slope and relief exhibit a trend toward steeper terrains including areas with near-vertical rockwalls, which are prominent in the upper portion of the basin (Figure S14 in the Supporting Information). For the four analyzed variables (elevation, permafrost, slope, and relief), exceptions exist for the year 1987 and the period between 2011 and 2016, which on average exhibit lower values than other periods (Supporting Information, Section S6).

By analyzing the lithology and geomorphology of the source locations we found that detachment points are equally distributed between metamorphic and sedimentary rocks (192 vs. 200 points respectively, with an overall point density of 21 pts/km^2), amounting to 38.5% of all instabilities (although divided between rockwalls [steepness $\geq 45°$] and bedrock outcrops [steepness $< 45°$], following the classification of Buter et al., 2020), whereas the majority of the detachments occur in unconsolidated Quaternary deposits (625 points, equal to 61.5%, with a point density of 11 pts/km^2). Considering that sedimentary rocks cover a smaller area of the basin, an analysis based on point density (i.e., the number of detachment points per unit area) indicated that sedimentary units contribute at least 35% more to the overall instability than metamorphic units (with a point density of 27 pts/km^2 compared to 17 pts/km^2 of the metamorphic rocks). A closer look at the morphological analysis reveals that rockwalls and bedrock outcrops constitute by far – in absolute terms – the most important sources for instability, followed by areas of diffuse erosion and shallow soils, unconsolidated sediment, and debris-flow channels (Figure 4a). This is generally true for all periods analyzed, except for 1987 and the period between 2011 and 2016 (Figure 4b). The situation changes
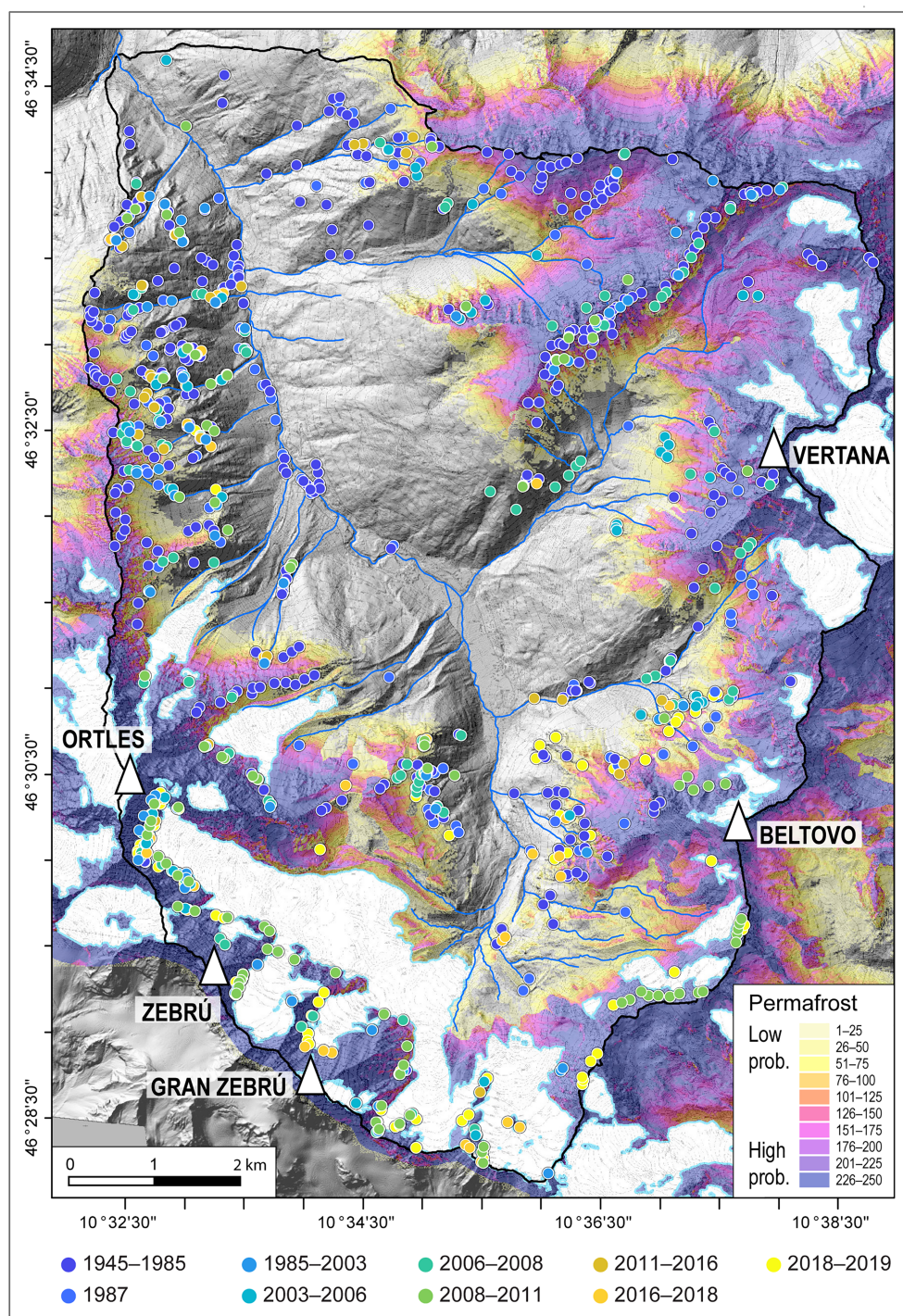
slightly when considering the areal extent of the different geomorphic domains, with areas of diffuse erosion, rockwalls, and bedrock characterized by a point density of 43 pts/km^2 versus 21 pts/km^2, and debris-flow channels by a point density of 16 pts/km^2. Unconsolidated material and shallow soils follow with a point density of 4 and 2 pts/km^2, respectively. Additional analyses indicate that 60.6% of the detachments (616 points, with a density of 14 pts/km^2) are located in areas with possible permafrost (i.e., permafrost probability > 0); 27.8% (283 points) are in areas that were already unstable (this category includes several geomorphic domains and a point density could not be retrieved); and 13.6% (136 points, density of 118 pts/km^2) are within areas that were recently exposed by ice retreat (i.e., had previously been covered by glaciers as

documented on the orthophotos of the earlier time frame). Only 4.3% of the detachment points (44 points, density of less than 1 pts/km^2) were subsequently stabilized by forest (see Figure S15 in the Supporting Information). It is interesting to note that most detachment points coincide with locations along channels and avalanche tracks (see Figure S16 in the Supporting Information) or are located at the upper boundary between bedrock and glacial ice (the point density in such newly exposed areas is three times higher compared to diffusive erosion areas, which is the second most active geomorphic domain). The processes at these locations appear to be strongly controlled by snow accumulation and ice melts, which influence the thermal properties of bedrock (see Sections 5.1 and 5.2), but glacial debuttressing may be an additional factor.
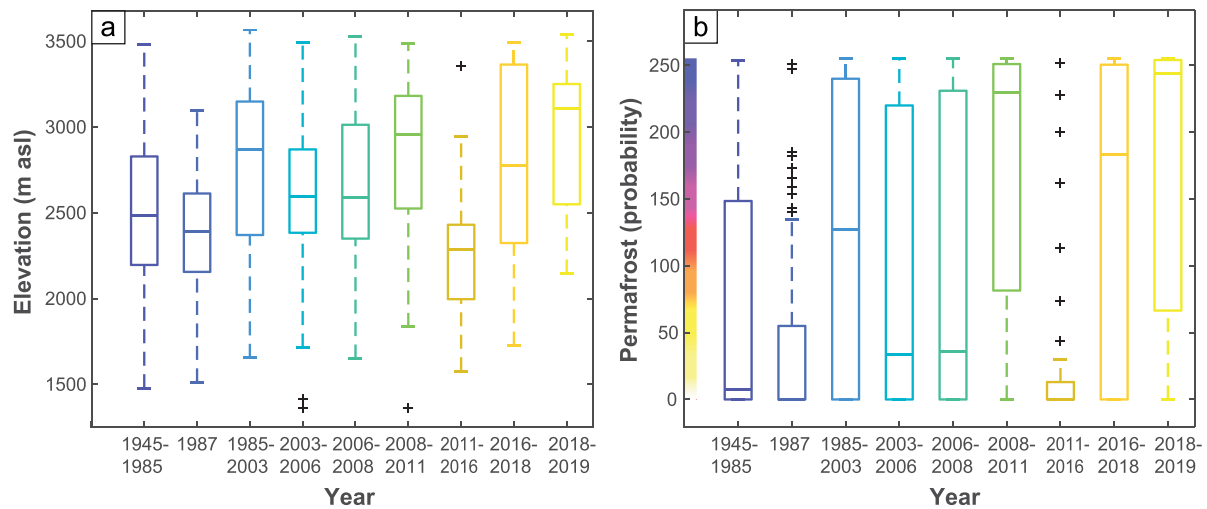
FIGURE 3 Variations in elevations (a) and permafrost probability (b) for the identified detachment points in the analyzed time periods. The graphs represent box plots with the median as central line, the 25th and 75th percentiles as bottom and top margins of the box, and ±2.7σ as the length of the whiskers (as the default calculation in Matlab). Black crosses are considered to be outliers [Color figure can be viewed at wileyonlinelibrary.com]

4.1.2 | Frequency of events

The total number of detachments detected for the time period 1945–1985 amounts to 404 events (i.e., an average of about 10 per year), compared to the 613 (18 per year) found in the period between 1985 and 2019, which suggests that instabilities and resulting failures have increased recently. However, the detachments identified in the period between 1945 and 1985 were likely underestimated. In fact, when using only the most recent orthophotos, thereby limiting the analysis to after 1985, no clear trend can be established (Table 1).

4.2 | Climatic analysis

4.2.1 | Trends, anomalies and extremes

Since 1955, the MAAT has been rising at both stations and for all seasons (Figure 5a; Supporting Information Figure S8 and Section S7). Warming has been more pronounced at higher elevations (i.e., at the Madritsch station) and during summer and spring. The analysis of the MAAT from 2010 to 2019 indicates for both stations a thermal anomaly of +1°C when compared to the period 1981–2010, and of +1.7°C and +2.6°C (for Sulden and Madritsch, respectively) when compared to the reference period 1961–1990 (Supporting Information Table S10). Differences can also be observed in seasonal anomalies (Figure 5a) with warm winters increasing in frequency starting in the late 1980s, and the other seasons showing a general warming phase starting from the early 2000s or later (Figures S11 and S12 and Section S7 of the Supporting Information).

Temperature extremes record a clear increase that can be observed at both stations and for all seasons (Figure 6; Supporting Information Figure S11 and Table S12). Overall, the year 2015 is the hottest year (with a MAAT = 4.9°C at Sulden and −0.5°C at Madritsch) and has had by far the highest number of extremely high daily temperatures (i.e., 72 days compared to an average of 18 d/yr; Table S11 in the Supporting Information). Important differences exist

at the seasonal scale (Table S12) and for different years. For example, while 2015 was associated with the highest number of hot days in summer, autumn, and particularly winter, the greater number of days with high temperatures in spring was registered in 2007. Also, summer and autumn months show a larger number of days with high temperatures at high altitudes (Madritsch station) compared to low elevations (Sulden station), but seasonal (Table S11) and annual differences do exist (Figure 6).

In contrast, the MAP showed no clear trends, although the period between 1996 and 2009 seems to have been drier than on average (Figure 5b; Supporting Information Table S8). When looking at seasonal trends, we observe that since 1987 (first year of measurement), precipitation has increased in all seasons except summer, which shows a slight decrease in monthly mean values (Figure 5b; Supporting Information Figure S9 and Table S8). Moreover, we have noticed generally drier periods from 1996/1997 to 2007/2008 for winter and spring, and from 2001/2002 to 2009/2010 for summer and autumn (Figure S11). At higher altitudes (e.g., Madritsch station), seasonal values show a positive trend in spring and summer, and negative trends in autumn and winter (Table S8).

4.2.2 | Rainfall events and debris-flow triggers

The analysis of all rainfall events in the Sulden basin since 1987 (see Section S3 of the Supporting Information) revealed that debris flows were triggered during rainstorms exceeding the 75th percentile of the entire distribution in terms of intensity and duration (CNR-IRPI, 2010; Nikolopoulos et al., 2015; Berti et al., 2020; Gregoretti & Dalla Fontana, 2007; see Figure S4 of the Supporting Information). Although a general clustering of high-intensity events during summer and long-duration events in autumn is seen (not shown here), most of the rainfall events strong enough to trigger debris flows generally occur in summer (July and August, Figure 7a). Their temporal evolution shows no particular trend, but highlights that the drier period between 1995 and 2009 was also characterized by a low number of intense rainfall events (Figures 7b).
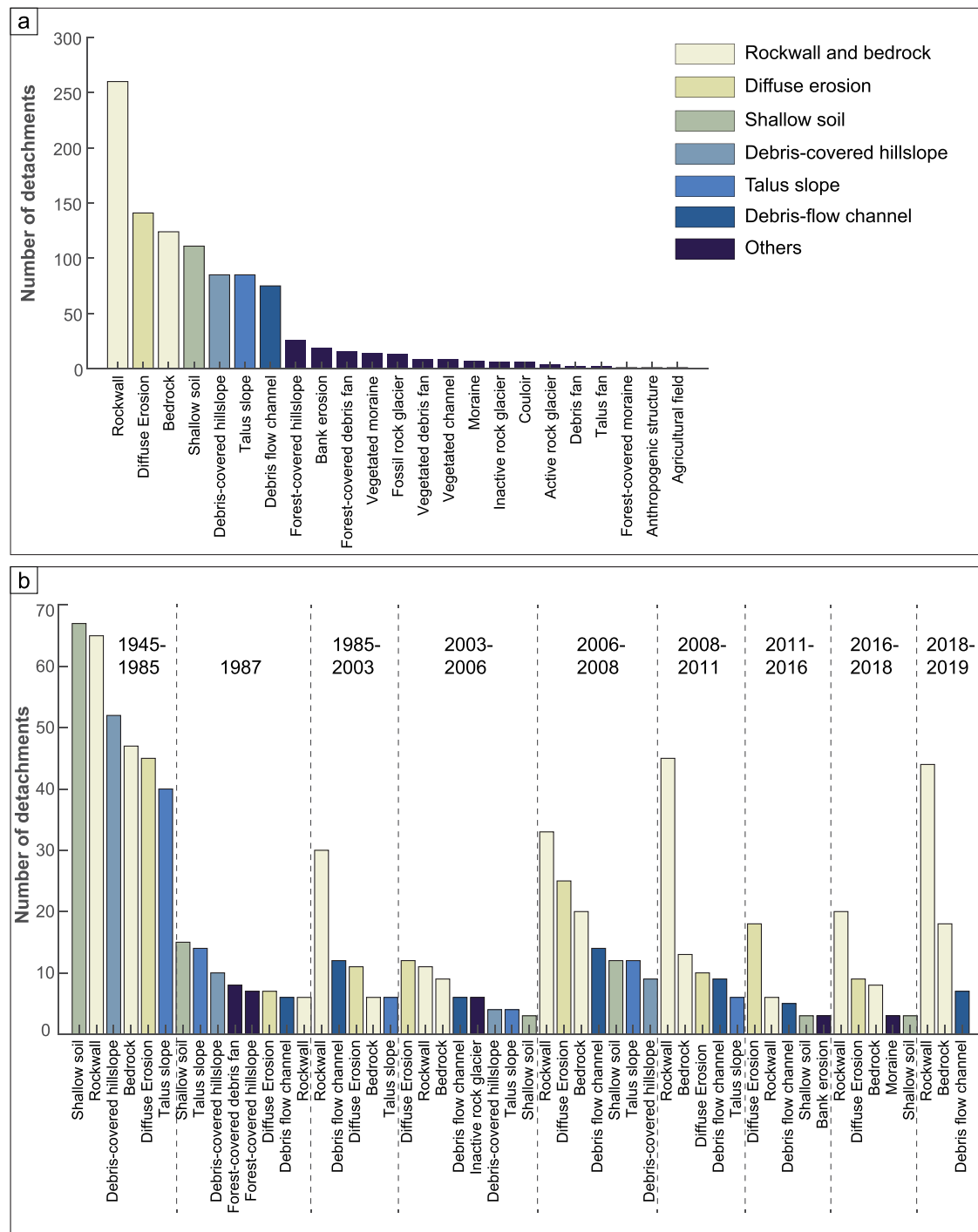
FIGURE 4 Number of detachments in each landform type (based on the geomorphic map of Buter *et al.*, 2020): (a) all detachment points; (b) detachment points sorted by time period (only landforms with more than 5% of detachments are shown) [Color figure can be viewed at wileyonlinelibrary.com]

TABLE 1 Number of detachments, rainfall events that triggered a debris flow, and debris flows, together with the detachment (Det.) and debris-flow (D-F) rates calculated annually

| Time periods	Detachments	Rainfall	Debris flows	Det. rate (number/yr)	D-F rate (number/yr)
1985–2003	158	5	14	8.8	0.8
2003–2006	58			19.3	0.7
2006–2008	132			66.0	
2008–2011	92			30.7	
2011–2016	43	4	12	8.6	2.4
2016–2018	49	1	1	24.5	0.5
2018–2019	81	2	3	81.0	3.0
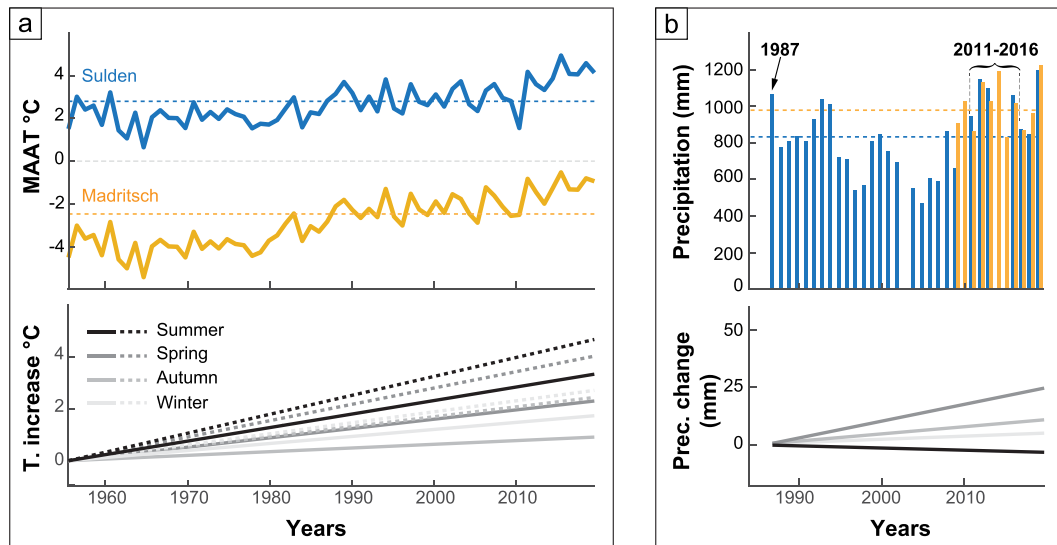
FIGURE 5 (a) Mean annual air temperature for Sulden and Madritsch stations (upper panel) with seasonal linear trends obtained by the "fit" Matlab algorithm (lower panel). In the upper panel, dotted lines represent the climatic reference MAAT (1981–2010; 3PClim database). In the lower panel, dotted lines represent measurements at Madritsch station, whereas continuous lines show measurements at Sulden. (b) Cumulative annual precipitation for the two stations (upper panel), with seasonal linear trends valid for the Sulden station only (lower panel). Colors follow the same scheme as in (a) [Color figure can be viewed at wileyonlinelibrary.com]
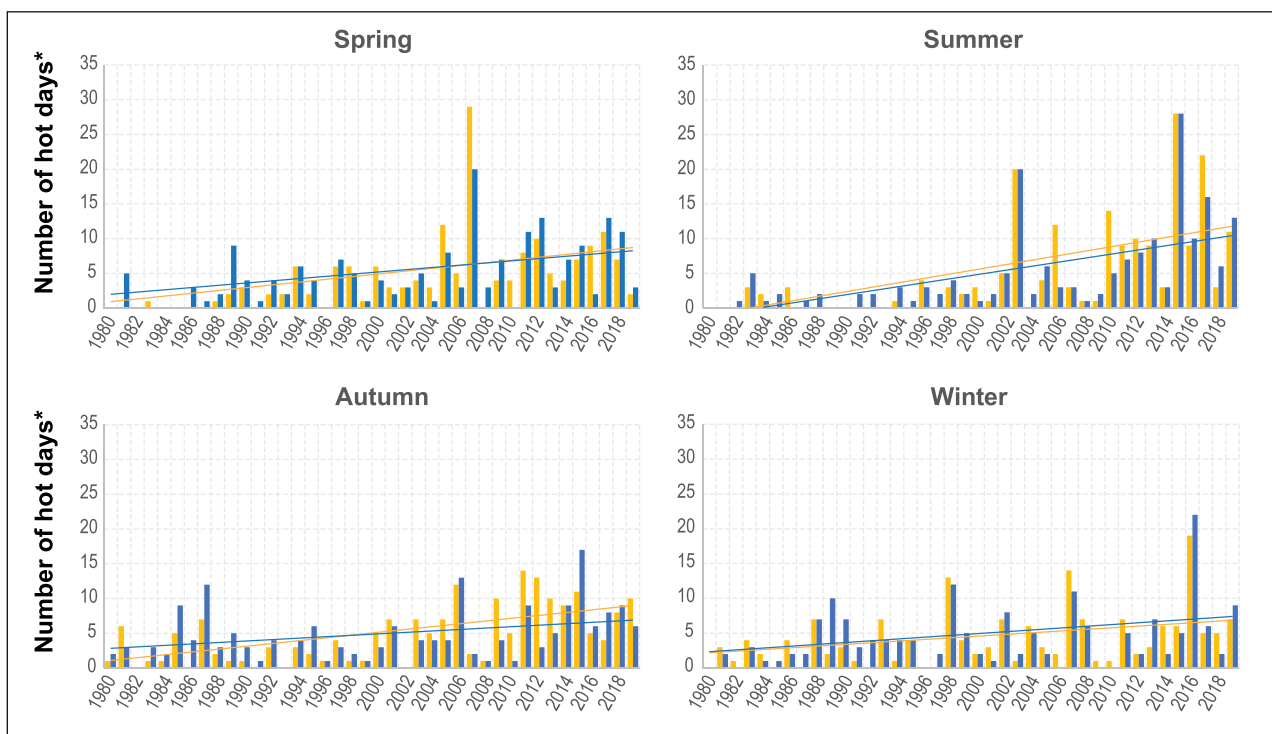
FIGURE 6 Number of hot days per season, that is, days with a mean temperature > 95th percentile of the reference daily temperatures for the time period 1980–2019 (e.g., time series with daily resolution) at both stations (colors follow the scheme as in Figure 5). Continuous lines represent linear trends [Color figure can be viewed at wileyonlinelibrary.com]

When cross-checking the data on rainfall, temperature, snow height, and snow cover (during the precipitation event and for 5 days prior to it, not shown here), we observed that in addition to rainfall intensity and duration, debris flows occurred only when the rainfall event was characterized by a constant warm air temperature. This promoted liquid precipitation also at high elevation, enhancing rain-on-snow effects and the melting of glacial ice (as already reported by

Schiona [1994] for events in 1987). Moreover, during these debris-flow triggering events, rainfall continued almost uninterruptedly with sustained high intensity, likely promoting rapid ground saturation. In addition, snow-cover extent was generally at its minimum (ca. 25% of the basin area), suggesting that fresh snow existed only on glaciers and in perennial snow patches. In contrast, other rainfall events with similar intensity and duration that did not trigger a debris flow were
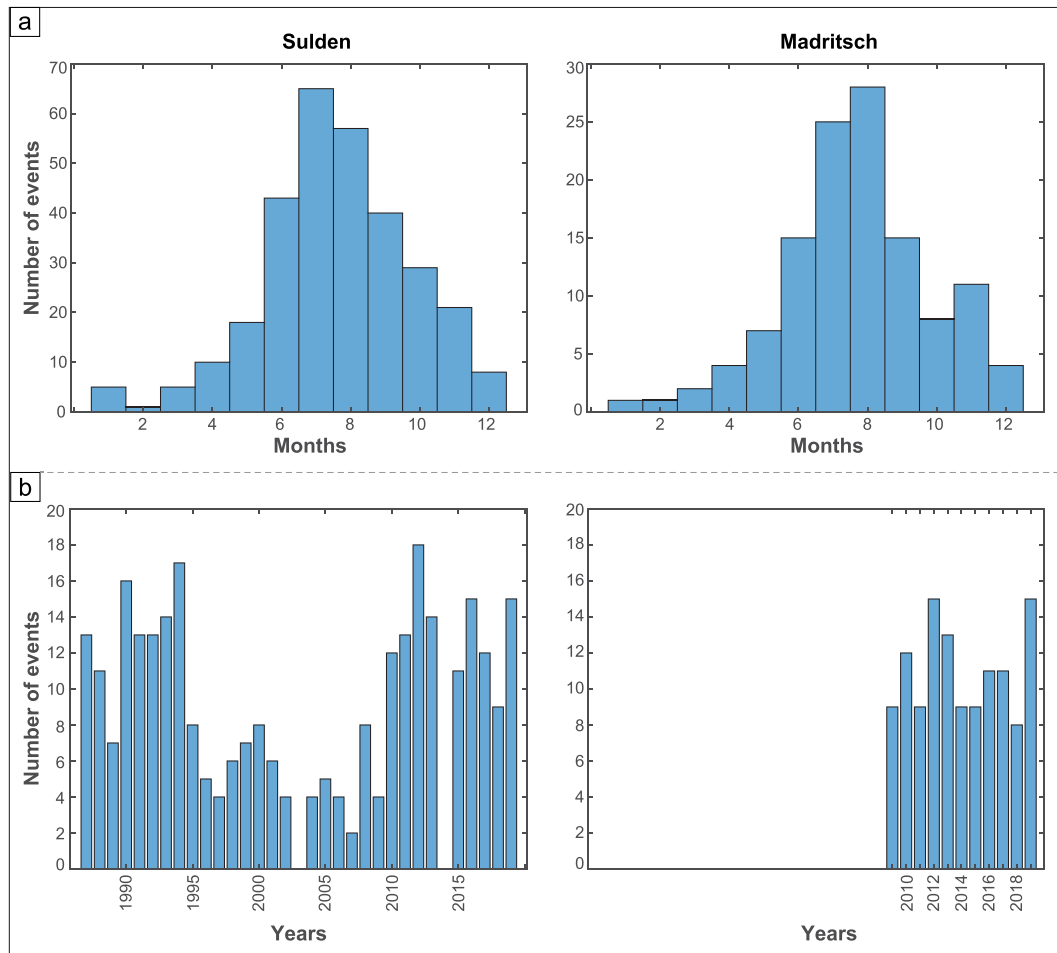
FIGURE 7 Analysis of rainfall events above the 75th percentile of the I-D distribution. (a) Monthly distribution of the events for the Sulden (left) and Madritsch (right) stations; (b) temporal evolution of rainfall events [Color figure can be viewed at wileyonlinelibrary.com]

characterized by: (i) a sudden drop in temperature at the beginning of the rainfall event, likely associated with cold fronts typical of advective storms, and (ii) irregular rainfall rates, which may have reduced the accumulation of surficial runoff (Berti et al., 2020) and the degree of ground saturation.

4.3 | Snow-cover effects on slope instability and results of frost-cracking modeling

Data on snow height, used to evaluate changes in snow-cover duration and snow-water equivalent (calculated based on the algorithm of Hill et al., 2019), showed no significant temporal trends for either of the two variables (Table S9 and Figure S10 in the Supporting Information). Implementing the approach of Draebing et al. (2014), we determined the most probable instability window for the Sulden basin based on snow-height measurements (Figure 8). With average snow conditions (i.e., averaged daily snow height for the measured period), at an elevation of ca. 2800 m (i.e., altitude of the Madritsch weather station), the ground can be considered snow-insulated from late November to early June (Figure 8a). Considering the combined effect of the different heat-transport modes (Figure 8b), the most probable instability window for the Sulden basin was found to occur in late spring (i.e., during snowmelt). Despite the absence of a temporal trend in snow-cover length, the yearly differences in snow height and

snow-cover duration have a large impact on the instability window, which can vary significantly from year to year. As an example, Figure 8c portrays the wide instability window of 2007 that resulted from the limited snow cover and extremely high temperatures characterizing the spring season in that year. Therefore, the high number of detachments observed in the period 2006–2008 may be ascribed to such an anomaly in 2007 (Table 1).

Figure S17 in the Supporting Information illustrates the intensity of frost cracking in the bedrock portions of the Sulden basin, based on the model described in Section 3.4. The outcome of the modeling indicates that cracking intensities at the location of the detachment points did not significantly vary through time (see Section S6 of the Supporting Information), and that at these locations the most intense frost cracking (defined as the mean FCI value > 90th percentile) occurred within 1 m depth. An exception is the 2008–2011 period, which shows intense FCI in average at greater depths (Figure 9).

5 | DISCUSSION

5.1 | Altitudinal and morphological distribution of detachment points

The spatiotemporal distribution of the detachment points in the Sulden basin mapped for the period 1945–2019 reveals how slope
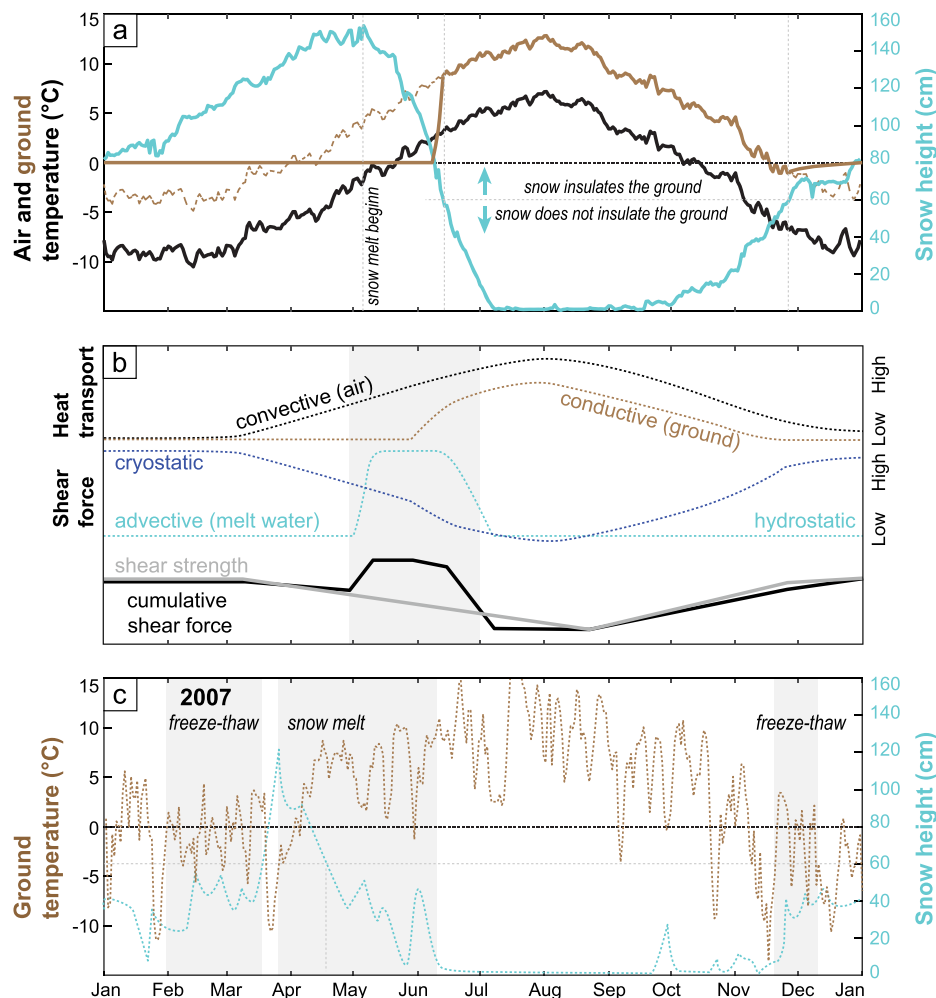
FIGURE 8 Variations of shear force and shear strength with associated "instability window" through an average year (a) in the Sulden basin (following the approach of Draebing *et al.*, 2014). Areas with gray shading in (b) and (c) represent the timing of most probable instability. In average, this timing occurs at the end of spring/beginning of summer, between May and June (b). Strong differences can, however, exist from year to year, depending on temperatures and snow cover conditions. In 2007, for example, the instability window was much wider, starting already in February and terminating at the beginning of June (c). In February and March, a thin snow cover (<60 cm) did not guarantee the insulation of the ground, which was subject to air-temperature fluctuations. As a consequence, snow and ice melt within the ground were influenced by freeze-and-thaw cycles and may have promoted instability. Subsequently, due to particularly warm temperatures, snow melt started early in April, extending the instability window until the beginning of June (end of snow melt). Also, particularly mild temperatures at the end of November, associated with a thin snow cover, may have created another instability window where ground temperatures promoted freeze-and-thaw conditions and instability [Color figure can be viewed at wileyonlinelibrary.com]

instability has shifted toward higher elevations over time (Figures 2 and 3; Section S6 in the Supporting Information), matching observations made in other studies in the Alps (e.g., Fischer et al., 2012; Ravanel et al., 2010; Ravanel & Deline, 2011). Also, in agreement with Hartmeyer et al. (2020), most detachments at high elevations (e.g., above 2500–2600 m a.s.l.) occurred along channels and avalanche tracks as well as in areas where glacial ice had recently vanished. Here, the recently exposed bedrock is suddenly subjected to daily and seasonal temperature variations (Fischer et al., 2006, 2012; Huggel et al., 2012; Wegmann et al., 1998) and thus to higher thermal stresses that may increase its susceptibility to rock breakdown. In channels and chutes, snow tends to accumulate providing abundant liquid water during snowmelt. In turn, this favors deep water percolation that enhances frost cracking and hydrothermal stresses, which may lead to bedrock failure (Deline et al., 2015; Draebing et al., 2014; Girard et al., 2013; Hartmeyer et al., 2020; Hasler et al., 2012). Unfortunately, the role of glacial debuttressing is difficult to evaluate in our study area. Deep-

seated landslides that may be related to this phenomenon have not been officially reported, but a partial influence of lateral stress variations on slope failure due to deglaciation is likely in the freshly-exposed bedrock areas (e.g., Johnston et al., 1998).

The analysis of landforms associated with slope instability highlights the predominant occurrence of bedrock failures for all time periods, except for the year 1987 and the period between 2011 and 2016 (Figure 4). It should be noted that these years were characterized by high amounts of precipitation (Figure 5b), with several rainfall events (Figure 7b) that triggered diffuse instability in several parts of the basin (Figure 1d).

Our results suggest that, whereas temperature-related processes such as frost cracking and the build-up of hydrothermal stress may be crucial prerequisites for rock failures, especially in sedimentary rocks, which are more susceptible to thermal variations and ice-segregation processes (Akagawa & Fukuda, 1991; Draebing et al., 2014; Hasler et al., 2012; Matsuoka, 2001; Murton et al., 2001), extreme rainfall
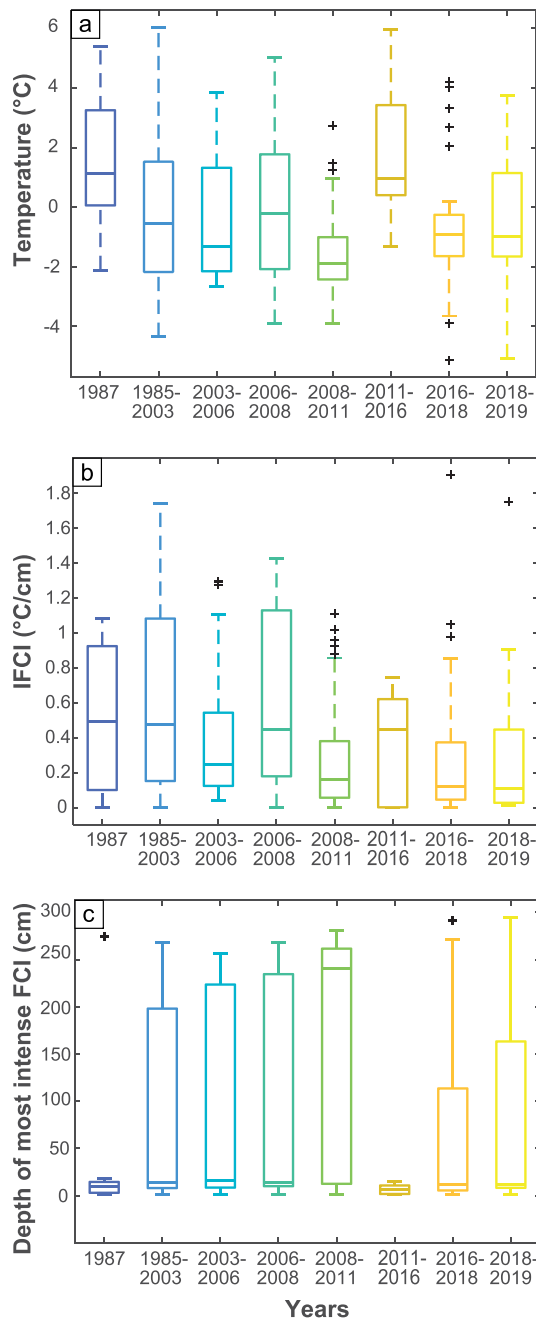
FIGURE 9 Mean annual ground-surface temperature (MAGST) (a), integrated frost-cracking intensity (IFCI) (b), and depth of most intense frost-cracking intensity (FCI) (c) calculated for the different time periods analyzed [Color figure can be viewed at wileyonlinelibrary.com]

events are responsible for a more diffusely distributed instability along rockwalls, areas of diffusive erosion, and debris-flow channels (see also Kofler et al., 2021). This may explain why during wetter periods, the elevation range, the potential occurrence of permafrost, slope, and relief of the detachment points were lower compared to other times (Figures 3 and S14).

Permafrost thawing is thought to be an important factor in causing not only rock failures but also shallow landslides on debris-covered areas (see also Kofler et al., 2021), as supported by our field observations of ice in landslide scars. Other researchers have noted that, in areas that were already unstable, instability may evolve independently from climatic conditions (Crozier, 2010; Fischer et al., 2012; Huggel et al., 2012), and detachments may be triggered

by less intense rainfall events (Crozier, 2010; Stoffel & Huggel, 2012; Stoffel et al., 2011). This appears to be the case with two small debris flows generated in the area of the tributary hosting the End of the World glacier during 2015 and 2016 (Figure 1c,d), which followed the destabilization of a rock-glacier front in 2014 (Kofler et al., 2021).

5.2 | Effects of temperatures and snow cover on frost-cracking processes and slope stability

Among other influencing factors, frost cracking is controlled by the MAGST and the daily temperature amplitude. For the Sulden basin, frost cracking occurs only when ground-surface temperatures are between +4°C and −7°C (Supporting Information Table S3). For temperatures above 4°C, the below-surface temperature is always positive, preventing water from freezing; for temperatures below −7°C, the below-surface temperature is always negative, preventing ice from melting. By observing the depth at which frost cracking is likely to occur, we noted that there is a sudden shift to deeper layers when the temperature passes from −1.5°C to −2°C (Table S3). Above this temperature, the average depth at which the most intense frost-cracking occurs is 10 cm, whereas below this temperature it is 2.55 m. Interestingly, this temperature range also marks a change in stability of ice-filled bedrock joints (Davies et al., 2001), and it is just below that of the freezing point for water in bedrock, which may promote important changes in hydraulic permeability and fluid pressures that act on small fractures in bedrock (Deline et al., 2015; Draebing & Krautblatter, 2019; Girard et al., 2013; Haeberli et al., 2010; Krautblatter, 2009; Krautblatter et al., 2013; Murton et al., 2001). As we have analyzed only small- to medium-sized events, this observation is important, because it reveals the temperature range that influences slope stability with respect to shallow failures, namely between +4°C and −2°C. Conditions promoting frost cracking close to the surface have not changed over time, but rising temperatures have shifted upward the altitudinal range where superficial frost cracking (i.e., at depths < 1 m) is most efficient.

An additional confirmation of the importance of temperature in the destabilization of rockwalls and bedrock outcrops is provided by the close correspondence between the number of detachments registered during the 2006–2008 period (Table 1) and the high number of days with extremely high temperatures registered in spring 2007 (Figure 6). The combination of various factors, including the effects of snow cover and snow melt on the thermal properties of the ground, was responsible for an extended period of instability that likely triggered the high number of detachments (Figure 8c; Hasler et al., 2012; Kofler et al., 2021; Matsuoka, 2001).

Besides providing water during snow melt, snow cover may affect permafrost thaw and the intensity of frost cracking by changing ground thermal conditions (Anderson et al., 2013; Girard et al., 2013; Draebing & Krautblatter, 2019; Harris & Conte, 1992). When snow cover has a thickness > 60 cm, it may insulate the ground from thermal variations (Luetschg & Haeberli, 2005; Noetzli & Gruber, 2009; Staub & Delaloye, 2017; Zhang, 2005), maintaining it at a constant temperature around 0°C (Anderson et al., 2013; Zhang, 2005). As such, a thick, extensive, and patchy snow cover may increase the thickness of the permafrost active layer (Draebing et al., 2017a; Huggel et al., 2012; Ravanel et al., 2013) by extending the duration at

which the ground is subject to melting conditions (Kofler et al., 2021). This may facilitate ground saturation during prolonged or intense rainfall events, thus preparing the slope for possible failure (Kofler et al., 2021). In contrast on surfaces with thick snow cover, frost cracking is reduced, if not eliminated, in the presence of a positive thermal gradient that limits cryosuction from depth (Draebing et al., 2017a; Supporting Information Figure S18). Slope stability is thus affected in two ways: Firstly, frost-cracking is limited to areas with thin (e.g., <60 cm) or no snow cover (e.g., low altitudes or steep rockwalls; Figure 10), whereas permafrost thaw may increase in areas with thick and prolonged snow accumulation. Secondly, snow cover may greatly contribute to future changes in slope stability depending on the evolution of temperatures and precipitation, which ultimately controls the amount of snowfall and duration of snow cover (Figure S18).

5.3 | Effects of recent climate warming

Intra-annual variations in either the development of detachment points or the generation of debris-flow events are difficult to assess (Table 1). Nevertheless, with a synoptic view of the changes that have occurred on a decadal timescale, some relevant observations can be made (Table 2). Particularly striking are the recent changes in temperature, with a significant increase in both mean annual values and in the number of days with extremely high temperatures. This latter parameter suggests that higher elevations have been subjected to an intense phase of warming, which had already started in the year 2000. Indeed, the number of days with high temperatures registered at the Madritsch station during the period between 2000 and 2009 is more than double than those during the previous decade. A similar increase was registered at Sulden one decade later (i.e., 2010–2019 compared to 2010–2009). Along with the rise in temperature during the 2000s, we observed a pronounced increase in the number of detachments. This correspondence in timing corroborates our finding that, in the context of warming, rock failures are a very important phenomena at high elevations, supporting the hypothesis that temperature-dominated processes (i.e., frost cracking, the build-up of hydrothermal stress, and permafrost thaw) are the main factors responsible for causing instability.

In contrast, wetter conditions during the past decade have had a more variable impact. Neither extreme rainfall events (i.e., above the
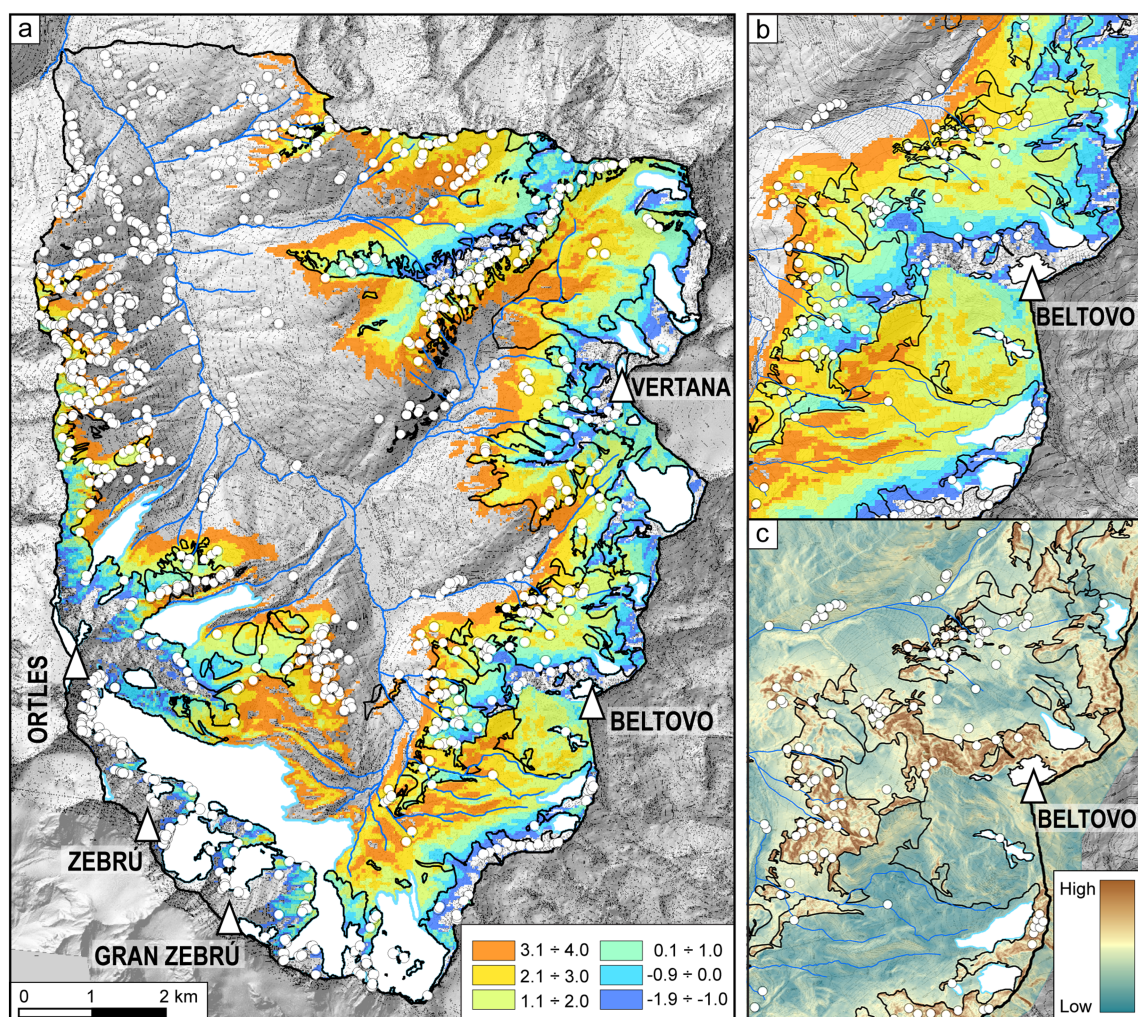
FIGURE 10 (a) Distribution of ground-surface temperatures ranging between +4°C and −2°C with superposed location of the detachment points (white circles; black line represents bedrock outcrops). (b) Enlarged view of the top of Beltovo: Note the lack of detachments in the bedrock areas with MAGST < −2°C (shown with no color along the ridges), where temperatures are too low to promote frost cracking at shallow depths. (c) Relief map: Note the lack of detachments where rock slopes are gentler (e.g., slope to the southwest of the Beltovo top) and snow can accumulate in thicker layers [Color figure can be viewed at wileyonlinelibrary.com]

75th percentile of the I-D distribution) nor rainfall events that triggered debris flows show any particular trends (Table 2). Nonetheless, during the last 10 years of our data set (2010–2019) the number of extreme rainfall events that have triggered debris flows has been higher than that of the previous three decades (i.e., seven vs. six events). Because the number of intense rainfall events has not significantly changed (Table 2), the increase in debris flows registered in the last 10 years may be related to the lack of events in the previous two decades (possibly associated with the drier 1995–2009 period), which led to an increased accumulation of unconsolidated debris at the potential initiation areas. Overall, this suggests that downstream sediment transport by debris-flow activity in the Sulden

TABLE 2 Decadal variations in temperature, precipitation, detachments, and debris-flow (D-F) events

	Temperature				Precipitation				Events		
	MAAT[a] (°C)		Tmean > 95th (days)		MAP[a] (mm)		Events > 75th		Number of detachment points	Number of rainfall events triggering D-F	Number of D-F
	S	M	S	M	S	M	S	M			
1980–1989	2.4	−3	107	59					94	4	12
1990–1999	2.8	−2.3	123	87	800.5		103		88	0	0
2000–2009	3	−2.1	178	222	606.1		45		151	2	2
2010–2019	3.8	−1.3	312	332	891.8	1016.2	123	112	175	7	16

[a]For comparison we report the values of the climatic reference time period 1981–2010. For Sulden (S): mean annual air temperature (MAAT) = 2.8°C, mean annual precipitation (MAP) = 835 mm; for Madritsch (M): MAAT = −2.4°C, MAP = 980 mm.
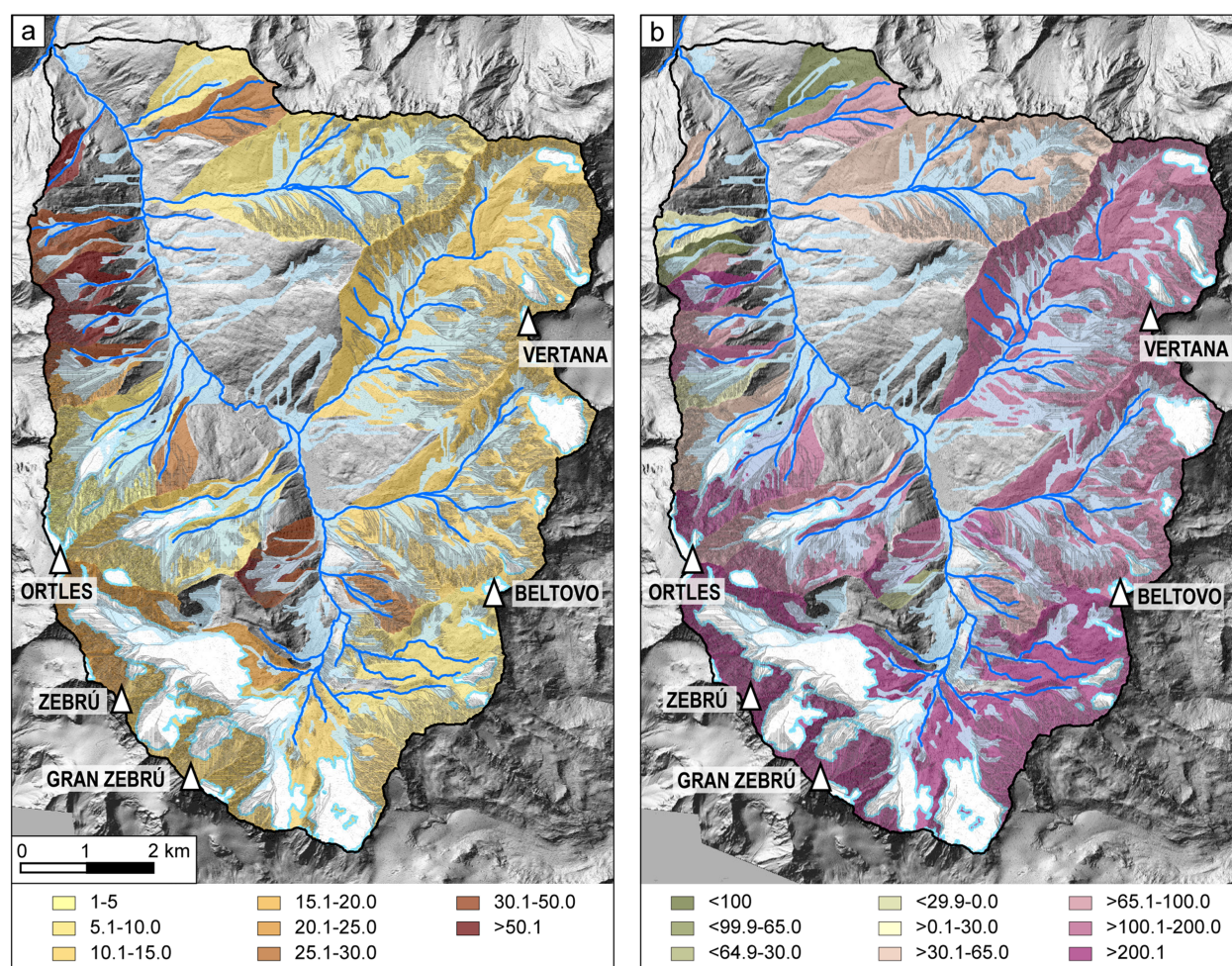
FIGURE 11 (a) Distribution of slope instability based on point density (e.g., number of detachments per square kilometer) and showed for single tributaries (for the whole time period analyzed: 1945–2019). (b) Percentage of change in point density between the time intervals 1985–2003 and 2003–2019, which span similar time intervals (i.e., 18 vs. 16 years). Olive-colored areas showed a reduction in instability (marked with the symbol < before the percentage class), whereas violet-colored zones exhibit an increase (marked with the symbol > before the percentage class). Rockfall trajectories are superposed on both images (thin lines in dark gray; Zischg, 2008; Zischg et al., 2012) with detachments starting in areas subjected to permafrost, and the areas at risk for debris flows (light blue; source: Autonomous Province of Bozen, 2011), which may indicate areas affected by possible cascading events [Color figure can be viewed at wileyonlinelibrary.com]

basin is limited to some extent by sediment availability and/or geo-morphic connectivity, as observed in several other Alpine mountain catchments (Buter, 2021; Marchi et al., 2019; Micheletti et al., 2015).

5.4 | Spatiotemporal variations in slope stability and consequences for management plans in Alpine regions

Using the point density as a metric for establishing the most unstable areas, we observed that major instabilities exist at the debris-flow tributaries on the north-western side of the basin (Figure 11a). Tem-poral variations of the detachment points (established by comparing the point density of the different areas between 1985–2003 and 2003–2019) indicate how instability has changed in the different trib-utaries, thus highlighting those events that have decreased or increased slope stability (Figure 11b). Increased instability has impacted the debris-flow tributaries to the northwest of the catch-ment as well as in the upper portion of the basin where rockwalls are most influenced by frost cracking, permafrost thaw, and receding gla-ciers. However, whereas debris-flow tributaries have also been active in the past, the upper portion of the basin has transitioned from a state of relative stability to one of relatively high instability (Figure 11).

Based on our findings, risk mitigation strategies in the Alps will need to focus in greater detail on the upper sectors of mountain basins, as events triggered at high elevations may promote hazardous cascading effects able to reach lower elevations (Beniston et al., 2018; Coe, 2020; Deline et al., 2015; Hock et al., 2019). To this end, it is essential to consider the degree of connectivity among the different geomorphic domains, as this parameter controls the amount of sedi-ments that can be transported to the valley bottom during changing meteorological conditions (Buter, 2021; Micheletti et al., 2015) and thus will influence the magnitude of future events. At the same time, the identification and mapping of possible rockfall and debris-flow runout areas (Autonomous Province of Bozen, 2011; Zischg, 2008; Zischg et al., 2012) expected along slopes in high-elevation sectors of mountain basins, will allow land managers to establish a sound, forward-looking hazard mapping (Figure 11).

6 | CONCLUSIONS

Our study clearly reveals a close relationship between current climatic warming and slope instability in a high-elevation catchment of the eastern Italian Alps. More specifically, we found that rockwalls and bedrock outcrops are the main source of instability, followed by areas of diffuse erosion and areas with debris-flow channels. At high eleva-tions, recently exposed rockwalls due to glacial retreat as well as channels and avalanche chutes where snow melt may have promoted severe frost cracking and hydrothermal stresses are particularly unsta-ble. These unstable sites may be further destabilized by low-intensity triggers, whereas slopes at lower elevation may be stabilized over time by the effect of colonizing vegetation.

Furthermore, temperature extremes are important for the genera-tion of detachments and, especially in late spring, contribute to rapid snowmelt and an increase in thickness of the active permafrost layer.

This, in turn, generates an "instability window," where failures can more easily occur due to the presence of liquid water percolating into rock fractures or saturating the ground. The rise in temperature affects the depth at which frost-cracking processes are most effec-tive; this causes shallow detachments in bedrock (depths < 1 m) to always occur at higher elevations where rockfalls are facilitated by precarious, steep rockwalls with weakened bedrock. In our study site, the location of detachment points has moved toward higher eleva-tions by ca. 300 m, and small- to medium-sized detachment events have increased in number since the beginning of the century, although with significant inter-annual variations.

Finally, rainfall events triggering debris flows have increased since 2010, most likely due to warmer and wetter summers. Although we did not observe a change in the frequency of extreme events, the sustained warm air temperatures typical of convective storms may have promoted rainfall not only in the lower portions of the basin, but also at high elevations, thus increasing runoff and ground saturation. In addition, the volume of weathered material produced during the previous two decades (1990–2009) has likely contributed to an increase in sediment availability and to its easier mobilization during subsequent wetter years, at least in those areas where sediment sources are directly connected to debris-flow channels.

In summary, the dynamic relationships between warming trends, permafrost degradation, changes in extreme rainfall events, and the occurrence of hazardous slope failures will be increasingly relevant for the higher sectors of Alpine catchments, if temperature levels remain elevated or increase further. Given the increased use of high-mountain areas for touristic purposes, future land management plans aimed at risk reduction must consider such effects of global warming that may cause significant changes in slope stability and potential cas-cading events.

CONFLICT OF INTEREST
We declare to have no conflict of interests.

DATA AVAILABILITY STATEMENT
All data used in this study can be requested to the corresponding author or to the relative authority (e.g., Province of Bolzano/Bozen).

ORCID

Sara Savi https://orcid.org/0000-0001-5515-753X

REFERENCES

3PClim. – Past, Present and Perspective Climate of Tirol, Südtirol-Alto Adige and Veneto. Available at: http://www.3pclim.eu/

Akagawa, S. & Fukuda, M. (1991) Frost heave mechanism in welded tuff. *Permafrost and Periglacial Processes*, 2(4), 301–309. https://doi.org/10.1002/ppp.3430020405

Allen, S. & Huggel, C. (2013) Extremely warm temperatures as a potential cause of recent high mountain rockfall. *Global and Planetary Change*, 107, 59–69. https://doi.org/10.1016/j.gloplacha.2013.04.007

Anderson, R.S., Anderson, S.P. & Tucker, G.E. (2013) Rock damage and regolith transport by frost: an example of climate modulation of the geomorphology of the critical zone. *Earth Surface Processes and Landforms*, 38(3), 299–316. https://doi.org/10.1002/esp.3330

Autonomous Province of Bolzano-Bozen. (2011) Ripartizione 30 - Opere idrauliche, Settore Sviluppo progetti: Carta indicativa del pericolo di colata detritica. Available at: http://geocatalogo.retecivica.bz.it/geokatalog/#!

Autonomous Province of Bolzano-Bozen. (2012) Ufficio idrografico: catasto dei ghiacciai 2006.

Ban, N., Schmidli, J. & Schär, C. (2015) Heavy precipitation in a changing climate: Does short-term summer precipitation increase faster? *Geophysical Research Letters*, 42(4), 1165–1172. https://doi.org/10.1002/2014GL062588

Barella, R., Callegari, M., Marin, C., Notarnicola, C., Zebisch, M., Sailer, R. et al. (2020) Automatic glacier outlines extraction from Sentinel-1 and Sentinel-2 time series. EGU General Assembly 2020, Online, 4–8 May 2020, EGU2020–13782. https://doi.org/10.5194/egusphere-egu2020-13782, 2020

Beniston, M., Farinotti, D., Stoffel, M., Andreassen, L.M., Coppola, E., Eckert, N. et al. (2018) The European mountain cryosphere: A review of its current state, trends, and future challenges. *The Cryosphere*, 12(2), 759–794. https://doi.org/10.5194/tc-12-759-2018

Berti, M., Bernard, M., Gregoretti, C. & Simoni, A. (2020) Physical interpretation of rainfall thresholds for runoff-generated debris flows. *Journal of Geophysical Research - Earth Surface*, 125, e2019JF005513. https://doi.org/10.1029/2019JF005513

Bertoldi, G., Notarnicola, C., Leitinger, G., Endrizzi, S., Zebisch, M., Della Chiesa, S. & Tappeiner, U. (2010) Topographical and eco-hydrological controls on land surface temperature in an Alpine catchment. *Ecohydrology*, 3, 189–204. https://doi.org/10.1002/eco.129

Boeckli, L., Brenning, A., Gruber, S. & Noetzli, J. (2012) Permafrost distribution in the European Alps: Calculation and evaluation of an index map and summary statistics. *The Cryosphere*, 6, 807–820. https://doi.org/10.5194/tc-6-807-2012

Bommer, C., Phillips, M. & Arenson, L. (2010) Practical recommendations for planning, constructing and maintaining infrastructure in mountain permafrost. *Short Communication, Permafrost and Periglacial Processes*, 21(1), 97–104. https://doi.org/10.1002/ppp.679

Buter, A. (2021) *Geomorphic connectivity and dynamics in an Alpine glacierised basin under different scenarios*. Bolzano, Italy: PhD Thesis, Free University of Bolzano.

Buter, A., Spitzer, A., Heckmann, T. & Comiti, F. (2020) A geomorphological map of the Sulden River basin (Italian Alps) for a sediment connectivity analysis. *Journal of Maps*, 16(2), 890–901. https://doi.org/10.1080/17445647.2020.1841036

Caine, N. (1980) The rainfall intensity – duration control of shallow landslides and debris flows. *Geografiska Annaler: Series A. Physical Geography*, 62(1–2), 23–27. https://doi.org/10.1080/04353676.1980.11879996

Carturan, L., Filippi, R., Seppi, R., Gabrielli, P., Notarnicola, C., Bertoldi, L. et al. (2013) Area and volume loss of the glaciers in the Ortles-Cevedale group (eastern Italian Alps): Controls and imbalance of the remaining glaciers. *The Cryosphere*, 7(5), 1339–1359. https://doi.org/10.5194/tc-7-1339-2013

Cavalli, M., Crema, S., Trevisani, S. & Marchi, L. (2017) GIS tools for preliminary debris-flow assessment at regional scale. *Journal of Mountain Science*, 14(12), 2498–2510. https://doi.org/10.1007/s11629-017-4573-y

CNR IRPI. (2010) Definizione di soglie di piovosità critica per l'innesco del debris flow di Cancia (Borca di Cadore, BL) - Convenzione tra l'AR-PAV ed il CNR-IRPI di Padova relativa ad un incarico di consulenza ed assistenza tecnico-scientifica per la realizzazione di un sistema di monitoraggio ed allarme in località Cancia del Comune di Borca di Cadore (BL).

Coe, J.A. (2020) Bellwether sites for evaluating changes in landslide frequency and magnitude in cryospheric mountainous terrain: A call for systematic, long-term observations to decipher the impact of climate change. *Landslides*, 17(11), 2483–2501. https://doi.org/10.1007/s10346-020-01462-y

Crespi, A., Matiu, M., Bertoldi, G., Petitta, M. & Zebisch, M. (2020) High-resolution daily series (1980–2018) and monthly climatologies (1981-2010) of mean temperature and precipitation for Trentino – South Tyrol (north-eastern Italian Alps). PANGAEA. https://doi.pangaea.de/10.1594/PANGAEA.924502 (dataset in review).

Crespi, A., Matiu, M., Bertoldi, G., Petitta, M. & Zebisch, M. (2021) A high-resolution gridded dataset of daily temperature and precipitation records (1980–2018) for Trentino – South Tyrol (north-eastern Italian Alps). *Earth System Science Data Discussions*. [preprint]. https://doi.org/10.5194/essd-2020-346

Crozier, M.J. (2010) Deciphering the effect of climate change on landslide activity: a review. *Geomorphology*, 124(3–4), 260–267. https://doi.org/10.1016/j.geomorph.2010.04.009

Damm, B. & Felderer, A. (2013) Impact of atmospheric warming on permafrost degradation and debris flow initiation – a case study from the eastern European Alps. *E&G Quaternary Science Journal*, 62(2), 136–149. https://doi.org/10.3285/eg.62.2.05

Davies, M.C., Hamza, O. & Harris, C. (2001) The effect of rise in mean annual temperature on the stability of rock slopes containing ice-filled discontinuities. *Permafrost and Periglacial Processes*, 12(1), 137–144. https://doi.org/10.1002/ppp.378

Deline, P., Gruber, S., Delaloye, R., Fischer L., Geertsema M., Giardino M. et al. (2015) Ice loss and slope stability in high-mountain regions. In: Haeberli, W. & Whiteman, C. (Eds.) *Snow and ice-related hazards, risks, and disasters*. Elsevier, Amsterdam, pp. 521–561, https://doi.org/10.1016/B978-0-12-394849-6.00015-9

Draebing, D., Haberkorn, A., Krautblatter, M., Kenner, R. & Phillips, M. (2017a) Thermal and mechanical responses resulting from spatial and temporal snow cover variability in permafrost rock slopes, Steintaelli, Swiss Alps. *Permafrost and Periglacial Processes*, 28(1), 140–157. https://doi.org/10.1002/ppp.1921

Draebing, D. & Krautblatter, M. (2019) The efficacy of frost weathering processes in Alpine rockwalls. *Geophysical Research Letters*, 46(12), 6516–6524. https://doi.org/10.1029/2019GL081981

Draebing, D., Krautblatter, M. & Dikau, R. (2014) Interaction of thermal and mechanical processes in steep permafrost rock walls: a conceptual approach. *Geomorphology*, 226, 226–235. https://doi.org/10.1016/j.geomorph.2014.08.009

Draebing, D., Krautblatter, M. & Hoffmann, T. (2017b) Thermo-cryogenic controls of fracture kinematics in permafrost rockwalls. *Geophysical Research Letters*, 44(8), 3535–3544. https://doi.org/10.1002/2016GL072050

Eisbacher, G.H. & Clague, J.J. (1984) Destructive mass movements in high mountains: Hazard and management. *Canadian Geotechnical Journal*, 22(3), 426–426. https://doi.org/10.1139/t85-060

Fischer, L., Kääb, A., Huggel, C. & Noetzli, J. (2006) Geology, glacier retreat and permafrost degradation as controlling factors of slope instabilities in a high mountain rock wall: The Monte Rosa east face. *Natural Hazards and Earth System Sciences*, 6(5), 761–772. https://doi.org/10.5194/nhess-6-761-2006

Fischer, L., Purves, R.S., Huggel, C., Noetzli, J. & Haeberli, W. (2012) On the influence of topographic, geological and cryospheric factors on rock avalanches and rockfalls in high-mountain areas. *Natural Hazards and Earth System Sciences*, 12(1), 241–254. https://doi.org/10.5194/nhess-12-241-2012

Girard, L., Gruber, S., Weber, S. & Beutel, J. (2013) Environmental controls of frost cracking revealed through in situ acoustic emission measurements in steep bedrock. *Geophysical Research Letters*, 40(9), 1748–1753. https://doi.org/10.1002/grl.50384

Gobiet, A., Kotlarski, S., Beniston, M., Heinrich, G., Rajczak, J. & Stoffel, M. (2014) 21st century climate change in the European Alps—a review. *Science of the Total Environment*, 493, 1138–1151. https://doi.org/10.1016/j.scitotenv.2013.07.050

Gregoretti, C. & Dalla Fontana, G. (2007) Rainfall threshold for the initiation of debris flows by channel-bed failure in the Dolomites. In: Chen, C.L. & Major, J.J. (Eds.) *Debris-Flow Hazards Mitigation: Mechanics, Prediction, and Assessment*. Rotterdam: Millpress, ISBN 978 90 5966 059 5.

Gruber, S., Hoelzle, M. & Haeberli, W. (2004a) Permafrost thaw and destabilization of Alpine rock walls in the hot summer of 2003. *Geophysical Research Letters*, 31(13), L13504. https://doi.org/10.1029/2004GL020051

Gruber, S., Hoelzle, M. & Haeberli, W. (2004b) Rock-wall temperatures in the Alps: Modelling their topographic distribution and regional differences. *Permafrost and Periglacial Processes*, 15(3), 299–307. https://doi.org/10.1002/ppp.501

Gubler, S., Endrizzi, S., Gruber, S. & Purves, R.S. (2013) Sensitivities and uncertainties of modeled ground temperatures in mountain environments. *Geoscientific Model Development*, 6(4), 1319–1336. https://doi.org/10.5194/gmd-6-1319-2013

Guzzetti, F., Peruccacci, S., Rossi, M. & Stark, C.P. (2007) Rainfall thresholds for the initiation of landslides in central and southern Europe. *Meteorology and Atmospheric Physics*, 98(3–4), 239–267. https://doi.org/10.1007/s00703-007-0262-7

Guzzetti, F., Peruccacci, S., Rossi, M. & Stark, C.P. (2008) The rainfall intensity–duration control of shallow landslides and debris flows: an update. *Landslides*, 5(1), 3–17. https://doi.org/10.1007/s10346-007-0112-1

Haeberli, W. (2013) Mountain permafrost — research frontiers and a special long-term challenge. *Cold Regions Science and Technology*, 96, 71–76. https://doi.org/10.1016/j.coldregions.2013.02.004

Haeberli, W. & Beniston, M. (1998) Climate change and its impacts on glaciers and permafrost in the Alps. In: Rapp, A. & Kessler, E. (Eds.) *Ambio – a journal of the human environment*, 4th edition. Stockholm: The Royal Swedish Academy of Sciences, pp. 258–265.

Haeberli, W., Huggel, C., Paul, F. & Zemp, M. (2013) Glacial responses to climate change. In: Shroder, J., John, F., James, L.A., Harden, C.P. & Clague, J.J. (Eds.) *Treatise on Geomorphology*. San Diego, CA: Elsevier, pp. 152–175.

Haeberli, W., Noetzli, J., Arenson, L., Delaloye, R., Gärtner-Roer, I., Gruber, S. et al. (2010) Mountain permafrost: Development and challenges of a young research field. *Journal of Glaciology*, 56(200), 1043–1058. https://doi.org/10.3189/002214311796406121

Haeberli, W., Wegmann, M. & Vonder Mühll, D. (1997) Slope stability problems related to glacier shrinkage and permafrost degradation in the Alps. *Eclogae Geologicae Helvetiae*, 90, 407–414.

Hales, T.C. & Roering, J.J. (2007) Climatic controls on frost cracking and implications for the evolution of bedrock landscapes. *Journal of Geophysical Research*, 112(F2), F02033. https://doi.org/10.1029/2006JF000616

Harris, S.A. & Conte, A.E. (1992) Interactions and relations between mountain permafrost, glaciers, snow and water. *Permafrost and Periglacial Processes*, 3(2), 103–110. https://doi.org/10.1002/ppp.3430030207

Hartmeyer, I., Delleske, R., Keuschnig, M., Krautblatter, M., Lang, A., Schrott, L. et al. (2020) Current glacier recession causes significant rockfall increase: The immediate paraglacial response of deglaciating cirque walls. *Earth Surface Dynamics*, 8, 729–751. https://doi.org/10.5194/esurf-8-729-2020

Hasler, A., Gruber, S. & Beutel, J. (2012) Kinematics of steep bedrock permafrost. *Journal of Geophysical Research – Earth Surface*, 117(F1), F01016. https://doi.org/10.1029/2011jf001981

Hasler, A., Gruber, S. & Haeberli, W. (2011) Temperature variability and offset in steep Alpine rock and ice faces. *The Cryosphere*, 5(4), 977–988. https://doi.org/10.5194/tc-5-977-2011

Hill, D.F., Burakowski, E.A., Crumley, R.L., Keon, J., Hu, J.M., Arendt, A.A. et al. (2019) Converting snow depth to snow water equivalent using climatological variables. *The Cryosphere*, 13(7), 1767–1784. https://doi.org/10.5194/tc-13-1767-2019

Hock, R., Rasul, G., Adler, C., Cáceres, B., Gruber, S., Hirabayashi, Y. et al. (2019) High mountain areas. In: Pörtner, H.-O., Roberts, D.C., Masson-Delmotte, V., Zhai, P., Tignor, M., Poloczanska, E. et al. (Eds.) *IPCC Special Report on the Ocean and Cryosphere in a Changing Climate*. In press.

Huggel, C., Allen, S., Deline, P., Fischer, L., Noetzli, J. & Ravanel, L. (2012) Ice thawing, mountains falling – are Alpine rock slope failures increasing? *Geology Today*, 28, 102–108.

IPCC. (2014) Climate Change 2014: Synthesis Report. In: Core Writing Team, Pachauri, R.K. & Meyer L.A. (Eds.) *Contribution of Working Groups I, II and III to the Fifth Assessment Report of the Intergovernmental Panel on Climate Change*. Geneva: IPCC, pp. 151.

ISPRA. (2012) *Carta Geologica d'Italia, Foglio Bormio*. Rome: SystemCart.

Jacob, D., Kotova, L., Teichmann, C., Sobolowski, S.P., Vautard, R., Donnelly, C. et al. (2018) Climate Impacts in Europe Under +1.5°C Global Warming. *Earth's Future*, 6(2), 264–285. https://doi.org/10.1002/2017EF000710

Johnston, P., Wu, P. & Lambeck, K. (1998) Dependence of horizontal stress magnitude on load dimension in glacial rebound models. *Geophysical Journal International*, 132(1), 41–60. https://doi.org/10.1046/j.1365-246x.1998.00387.x

Kofler, C., Mair, W., Gruber, S., Todisco, M.T., Nettleton, I., Steger, S. et al. (2021) When do rock glacier fronts collapse? Insights from two case studies in South Tyrol (Italian Alps). *Earth Surface Processes and Landforms*. https://doi.org/10.1002/esp.5099

Kofler, C., Steger, S., Mair, W., Zebisch, M., Comiti, F. & Schneiderbauer, S. (2020) An inventory-driven rock glacier status model (intact vs. relict) for South Tyrol, Eastern Italian Alps. *Geomorphology*, 350, 106887. https://doi.org/10.1016/j.geomorph.2019.106887

Krautblatter, M., (2009) Detection and quantification of permafrost change in Alpine rock walls and implications for rock instability. Bonn, Germany: PhD Thesis, University of Bonn.

Krautblatter, M., Funk, D. & Günzel, F.K. (2013) Why permafrost rocks become unstable: a rock-ice-mechanical model in time and space. *Earth Surface Processes and Landforms*, 38(8), 876–887. https://doi.org/10.1002/esp.3374

Krautblatter, M. & Moser, M. (2009) A nonlinear model coupling rockfall and rainfall intensity based on a four year measurement in a high Alpine rock wall (Reintal, German Alps). *Natural Hazards and Earth System Sciences*, 9(4), 1425–1432. https://doi.org/10.5194/nhess-9-1425-2009

Krautblatter, M., Moser, M., Schrott, L., Wolf, J. & Morche, D. (2012) Significance of rockfall magnitude and carbonate dissolution for rock slope erosion and geomorphic work on Alpine limestone cliffs (Reintal, German Alps). *Geomorphology*, 167, 21–34.

Li, A., Xia, C., Bao, C. & Yin, G. (2019) Using MODIS land surface temperatures for permafrost thermal modeling in Beiluhe Basin on the Qinghai-Tibet plateau. *Sensors*, 19(19), 4200. https://doi.org/10.3390/s19194200

Luetschg, M. & Haeberli, W. (2005) Permafrost evolution in the Swiss Alps in a changing climate and the role of the snow cover. *Norsk Geografisk Tidsskrift – Norwegian Journal of Geography*, 59(2), 78–83. https://doi.org/10.1080/00291950510020583

Marchi, L., Brunetti, M.T., Cavalli, M. & Crema, S. (2019) Debris-flow volumes in northeastern Italy: Relationship with drainage area and size probability. *Earth Surface Processes and Landforms*, 44(4), 933–943. https://doi.org/10.1002/esp.4546

Marchi, L., Cazorzi, F., Arattano, M., Cucchiaro, S., Cavalli, M. & Crema, S. (2020) Debris flows recorded in the Moscardo catchment (Italian Alps) between 1990 and 2019. *Natural Hazards and Earth System Science Discuss.*, 21(1), 87–97. https://doi.org/10.5194/nhess-2020-276

Matiu, M., Jacob, A. & Notarnicola, C. (2019) Daily MODIS snow cover maps for the European Alps from 2002 onwards at 250 m horizontal resolution along with a nearly cloud-free version. *Data*, 5(1), 1. https://doi.org/10.3390/data5010001

Matsuoka, N. (2001) Microgelivation versus macrogelivation: Toward bridging the gap between laboratory and field frost weathering. *Permafrost and Periglacial Processes*, 12(3), 299–313. https://doi.org/10.1002/ppp.393

Matsuoka, N., Hirakawa, K., Watanabe, T., Haeberli, W. & Keller, F. (1998) The role of diurnal, annual and millennial freeze–thaw cycles in controlling Alpine slope instability. Permafrost, Seventh International Conference Proceedings, Yellowknife, (Canada), Collection Nordicana, p. 55.

McColl, S.T., & Draebing, D. (2019) Rock slope instability in the proglacial zone: State of the art. In: Heckmann, T. & Morche, D. (Eds.), *Geomorphology of Proglacial Systems, Geography of the Physical Environment*. Cham: Springer Nature. https://doi.org/10.1007/978-3-319-94184-4_8

Micheletti, N., Lambiel, C. & Lane, S.N. (2015) Investigating decadal-scale geomorphic dynamics in an Alpine mountain setting. *Journal of Geophysical Research: Earth Surface*, 120(10), 2155–2175. https://doi.org/10.1002/2015JF003656

Mittal, A., Soundararajan, R. & Bovik, A.C. (2013) Making a completely blind image quality analyzer. *IEEE Signal Processing Letters*, 22(3), 209–212.

Müller, R., Behrendt, T., Hammer, A. & Kemper, A. (2012) A new algorithm for the satellite-based retrieval of solar surface irradiance in spectral bands. *Remote Sensing*, 4(3), 622–647. https://doi.org/10.3390/rs4030622

Murton, J., Coutard, J. & Lautridou, J. (2001) Physical modelling of bedrock brecciation by ice segregation in permafrost. *Permafrost and Periglacial Processes*, 12(3), 255–266. https://doi.org/10.1002/ppp.390

Murton, J.B., Peterson, R. & Ozouf, J. (2006) Bedrock fracture by ice segregation in cold regions. *Science*, 314(5802), 1127–1129. https://doi.org/10.1126/science.1132127

Nikolopoulos, E.I., Borga, M., Marra, F., Crema, S. & Marchi, L. (2015) Debris flows in the eastern Italian Alps: Seasonality and atmospheric circulation patterns. *Natural Hazards and Earth System Sciences*, 15(3), 647–656. https://doi.org/10.5194/nhess-15-647-2015

Noetzli, J. & Gruber, S. (2009) Transient thermal effects in Alpine permafrost. *The Cryosphere*, 3(1), 85–99. https://doi.org/10.5194/tc-3-85-2009

Notarnicola, C., Di Rosa, D. & Posa, F. (2011) Cross-comparison of MODIS and CloudSat data as a tool to validate local cloud cover masks. *Atmosphere*, 2(3), 242–255. https://doi.org/10.3390/atmos2030242

Notarnicola, C., Duguay, M., Moelg, N., Schellenberger, T., Tetzlaff, A., Monsorno, R. *et al*. (2013a) Snow cover maps from MODIS images at 250 m resolution, part 1: Algorithm description. *Remote Sensing*, 5(1), 110–126. https://doi.org/10.3390/rs5010110

Notarnicola, C., Duguay, M., Moelg, N., Schellenberger, T., Tetzlaff, A., Monsorno, R. *et al*. (2013b) Snow cover maps from MODIS images at 250 m resolution, part 1: Validation. *Remote Sensing*, 5(4), 1568–1587. https://doi.org/10.3390/rs5041568

Paranunzio, R., Chiarle, M., Laio, F., Nigrell, G., Turconi, L. & Luino, F. (2019) New insights in the relation between climate and slope failures at high-elevation sites. *Theoretical and Applied Climatology*, 137(3–4), 1765–1784. https://doi.org/10.1007/s00704-018-2673-4

Porter, S.C. & Orombelli, G. (1981) Alpine rockfall hazards: Recognition and dating of rockfall deposits in the western Italian Alps lead to an understanding of the potential hazards of giant rockfalls in mountainous regions. *American Scientist*, 69, 67–75.

Ravanel, L., Allignol, F., Deline, P., Gruber, S. & Ravello, M. (2010) Rock falls in the Mont Blanc Massif in 2007 and 2008. *Landslides*, 7(4), 493–501. https://doi.org/10.1007/s10346-010-0206-z

Ravanel, L. & Deline, P. (2011) Climate influence on rockfalls in high-Alpine steep rockwalls: The north side of the Aiguilles de Chamonix (Mont Blanc Massif) since the end of the 'Little Ice Age'. *The Holocene*, 21(2), 357–365. https://doi.org/10.1177/0959683610374887

Ravanel, L., Deline, P., Lambiel, C. & Vincent, C. (2013) Instability of a high Alpine rock ridge: The lower arête des cosmiques, Mont Blanc Massif, France. *Geografiska Annaler: Series A. Physical Geography*, 95(1), 51–66. https://doi.org/10.1111/geoa.12000

Rode, M., Schnepfleitner, H. & Sass, O. (2016) Simulation of moisture content in Alpine rockwalls during freeze–thaw events: Simulation of moisture content in Alpine rock walls. *Earth Surface Processes and Landforms*, 41(13), 1937–1950. https://doi.org/10.1002/esp.3961

Salzmann, N., Noetzli, J., Hauck, C., Gruber, S., Hoelzle, M. & Haeberli, W. (2007) Ground surface temperature scenarios in complex high-mountain topography based on regional climate model results. *Journal of Geophysical Research*, 112, F02S12. https://doi.org/10.1029/2006JF000527

Sánchez-Aparicio, M., Andrés-Anaya, P., Del Pozo, S. & Lagüela, S. (2020) Retrieving land surface temperature from satellite imagery with a novel combined strategy. *Remote Sensing*, 12(2), 277. https://doi.org/10.3390/rs12020277

Sass, O. & Oberlechner, M. (2012) Is climate change causing increased rockfall frequency in Austria? *Natural Hazards and Earth System Sciences*, 12(11), 3209–3216. https://doi.org/10.5194/nhess-12-3209-2012

Scherler, D. (2014) Climatic limits to headwall retreat in the Khumbu Himalaya, eastern Nepal. *Geology*, 42(11), 1019–1022. https://doi.org/10.1130/G35975.1

Schiona, A.S. (1994) *Gli eventi alluvionali dell'estate 1987 nelle valli di Solda e Trafoi*. Padua, Italy: Master Thesis, University of Padua, p. 140.

Schlögel, R., Kofler, C., Gariano, S.L., Van Campenhout, J. & Plummer, S. (2020) Changes in climate patterns and their association to natural hazard distribution in South Tyrol (eastern Italian Alps). *Scientific Reports*, 10(1), 5022. https://doi.org/10.1038/s41598-020-61615-w

Scorpio, V., Andreoli, A., Zaramella, M., Moritsch, S., Theule, J., Dell'Agnese, A. *et al*. (2020) Restoring a glacier-fed river: Past and present morphodynamics of a degraded channel in the Italian Alps. *Earth Surface Processes and Landforms*, 45(12), 2804–2823. https://doi.org/10.1002/esp.4931

Sobrino, J.A., Julien, Y. & García-Monteiro, S. (2020) Surface temperature of the planet earth from satellite data. *Remote Sensing*, 12(2), 218. https://doi.org/10.3390/rs12020218

Staub, B. & Delaloye, R. (2017) Using near-surface ground temperature data to derive snow insulation and melt indices for mountain permafrost applications. *Permafrost and Periglacial Processes*, 28(1), 237–248. https://doi.org/10.1002/ppp.1890

Stocker-Mittaz, C., Hoelzle, M. & Haeberli, W. (2002) Modelling Alpine permafrost distribution based on energy-balance data: A first step. *Permafrost and Periglacial Processes*, 13(4), 271–282. https://doi.org/10.1002/ppp.426

Stoffel, M., Bollschweiler, M. & Beniston, M. (2011) Rainfall characteristics for periglacial debris flows in the Swiss Alps: past incidences – potential future evolutions. *Climatic Change*, 105(1–2), 263–280. https://doi.org/10.1007/s10584-011-0036-6

Stoffel, M. & Huggel, C. (2012) Effects of climate change on mass movements in mountain environments. *Progress in Physical Geography*, 36(3), 421–439. https://doi.org/10.1177/0309133312441010

Stötter, J., (1994) Veränderungen der Kryosphäre in Vergangenheit und Zukunft sowie Folgeerscheinungen - Untersuchungen in ausgewählten Hochgebirgsräumen im Vinschgau (Südtirol). Unveröff. Habilitationsschrift, Fakultät für Geowissenschaften, Ludwig-Maximilians-Universität München, p. 285.

Valentini, P. (1985) Il catasto dei ghiacciai della provincia di Bolzano. *Geografia Fisica e Dinamica Quaternaria*, 8, 182–195.

Wegmann, M., Gudmundsson, G.H. & Haeberli, W. (1998) Permafrost changes in rock walls and the retreat of Alpine glaciers: A thermal modelling approach. *Permafrost and Periglacial Processes*, 9(1), 23–33. https://doi.org/10.1002/(SICI)1099-1530(199801/03)9:1<23::AID-PPP274>3.0.CO;2-Y

Zhang, T. (2005) Influence of the seasonal snow cover on the ground thermal regime: An overview. *Reviews of Geophysics*, 43(4), RG4002. https://doi.org/10.1029/2004RG000157

Zischg, A. (2008) Schutzwald-Hinweiskarte Südtirol. Endbericht Projekt APB Schutzwald, Amt für Forstplanung, Bozen.

Zischg, A., Mair, W. & Lang, K. (2012) PROALP – Kartierung und Monitoring von Permafrost in der Autonomen Provinz Bozen, Südtirol, Italien. 12th Congress INTERPRAEVENT 2012 – Grenoble/France Conference Proceedings

SUPPORTING INFORMATION

Additional supporting information may be found online in the Supporting Information section at the end of this article.